The degradation of electrospun polydioxanone patches for rotator cuff repair

Simon Hislop

Oriel College

Oxford University

MSc by Research: Musculoskeletal Sciences

Botnar Research Centre

Nuffield Orthopaedic Centre

Oxford University

Michaelmas 2012

Declaration

Work presented in this thesis was carried out solely by Simon Hislop, except the images in Figure 6 which were taken by Dr. Urszula Stacewitz, and the graphs and table in Figure 12, which were produced by Hamish Lowdon.

I would like to take this opportunity to thank Osnat Hakimi for being a fantastic supervisor with prodigious reserves of patience, tolerance and optimism, and Andy Carr for providing me with a wonderful opportunity and his on-going support and encouragement. I would also like to thank Stan Ng, Isaiah Adekanmbi, Tyler Grant, and Kalin Dragnevski for their invaluable help and technical input, and Afsie Sabokbar and Rich Murphy for their support and enthusiasm.

Table of Contents

Declaration 2

Acknowledgements 3

Table of Contents 4

Table of Figures 7

Abbreviations 11

1 Introduction 12

1.1 Background 12

1.1.1 Anatomy and pathology 12

1.1.2 Tendon repair implants 13

1.1.3 A fourth generation of rotator cuff repair? 14

1.2 Polydioxanone as a biomaterial 15

1.2.1 Polymers 15

1.2.2 Polydioxanone 16

1.2.3 Synthesis 17

1.2.4 Properties 18

1.2.5 Degradation 18

1.2.6 Tissue response 22

1.3 Cell recruitment and attachment 23

1.3.1 Mechanical properties 24

1.4 Potential for tissue engineering and Orthopaedic applications 25

1.5 Scope of study 25

2 Characterisation of novel PDO patches by electron and fluorescent microscopy 27

2.1 Introduction 27

2.2 Materials and Methods 29

2.2.1 Electrospinning of the polydioxanone patch prototype 29

2.2.2 Environmental Scanning Electron Microscopy 31

2.2.3 Fluorescence microscopy 32

2.3 Results 33
2.3.1 ESEM 33
2.3.2 Fluorescent Microscopy 40
2.4 Discussion 44
2.4.1 Further work 46
3 Monitoring the degradation of PDO patches using weight loss, pH and high performance liquid chromatography 47
3.1 Introduction 47
3.1.1 PDO degradation mechanism 47
3.1.2 Polydioxanone's final degradation product 50
3.1.3 High Performance Liquid Chromatography (HPLC) 51
3.1.4 Weight Loss and pH 55
3.1.5 Aim 57
3.2 Materials and Methods 58
3.2.1 Weight loss 58
3.2.2 pH 58
3.2.3 HPLC study to identify polydioxanone's final degradation product 59
3.2.4 Static and dynamic experiments 59
3.2.5 HPLC analysis: optimisation experiment 60
3.2.6 HPLC analysis: degradation kinetics experiment 61
3.2.7 HPLC analysis: calibration curve formation 63
3.2.8 HPLC analysis: dynamic and static experiments 65
3.2.9 Threshold of detection 67
3.3 Results 68
3.3.1 Weight loss 68
3.3.2 pH 69
3.3.3 Results of study to define polydioxanone's final degradation product 71
3.3.4 Results of HPLC optimisation study and degradation kinetics study 73

3.4 Discussion 76
3.4.1 Weight loss and pH 76
3.4.2 Degradation Mechanism using HPLC 77
3.4.3 Identifying the degradation product 80
3.4.4 Limitation 81
3.4.5 Further work 81
4 References 83

Table of Figures

Figure 1: The muscles of the rotator cuff viewed from posterior (left) and anterior (right). 12

Figure 2: Common methods of rotator cuff repairs such as standard double row suture fixation of sheep rotator cuff using non-degradeable Fibrewire sutures (A, O. Hakimi et al 2012, unpublished) and GraftJacket (B, Wright Medical) a de-cellularised skin matrix, thought to promote tissue growth (5). 14

Figure 3: The formation of the polydioxanone polymer from the p-dioxanone monomer. 16

Figure 4: Schematic of electrospinning apparatus. Boland et al (10) 17

Figure 5: The excretion of polydioxanone (11). 20

Figure 6: Electron micrographs showing randomly oriented electrospun polydioxanone fibres (A) and the variation in fibre diameter (B,C). Images courtesy of Dr. Urszula Stacewitz. 30

Figure 7: 'Bubbling' on the surface of (A) a PDSII suture and (B) a PDO electrospun patch. Note the crystals of salt visible in image A. 32

Figure 8: An un-degraded, gold-sputtered polydioxanone patch viewed in an ESEM. Of note are the long, continuous fibres that stretch across the patch (one in particular highlighted by black arrows. 35

Figure 9: ESEM images of fresh electrospun PDO patches. A, B, C, D and E show long continuous fibres running across the patches prior to degradation. Image B shows an undegraded PDO patch at 500x. This patch has had tensile stress exerted on it which manifests in less regular layering of fibres. All these samples were gold-sputtered. ... 36

Figure 10: ESEM images of electrospun PDO patches degraded in PBS for 30 days (A) or 56 days (B to G). Note the short chopped nature of the polymer fibres. After 30 days (A) surface erosion of the fibres has occurred, while after 56 days (B to G), deep and thorough degradation has affected all visible fibres. 37

Figure 11: ESEM images of electrospun PDO patches that have been seeded with tenoblasts and incubated for 42 days, showing the patch (E, F, G) as well as fragments which were seen around it (C, D, H). Red arrows point to cells. 38

Figure 12: Graphs and table to show the comparison of diameters of fibres of PDO measured in micrometres (µm) using ImageJ (National Institutes of Health, USA). Graph A shows data from the fresh patch while Graph B shows data from a patch degraded in PBS for 56 days. Figure 11C reveals that the diameters between the 2 time points are remarkably similar with the degraded fibres mean diameter, in fact, being slightly larger. 40

Figure 13: Tenoblasts incorporated into the PDO patch viewed after 4 weeks in culture. The white arrow points to a cell body. 42

Figure 14: Cells stained red and visible on the degraded PDO patch at 4 weeks (10x). 43

Figure 15: Tenoblasts on a PDO patch degraded for 4 weeks and stained with DAPI (20x). The cells can be seen as brighter areas, and the broken ends of fibres are visible. This corresponds to the degradation pattern seen in the ESEM images of degraded fibres. Figure 14B: After 1 week x20 DAPI stain: showing cells attached to a fragment that has broken off from the main body of the patch. 44

Figure 16: Proposed approximate model of the detailed degradation of PDO (This figure is courtesy of Sabino *et al* and contains modifications) (15). 49

Figure 17: The chemical structure of lactic acid, glycolic acid and glyoxylic acid. 51

Figure 18: A schematic representation of an HPLC apparatus. Figure courtesy of https://waters.com/waters/nav.htm?cid=10049055 53

Figure 19: A schematic representation of compounds passing through an HPLC column and being separated according to their affinity to the static phase. Figure courtesy of https://waters.com/waters/nav.htm?cid=10049055. 53

Figure 20: An example of a chromatogram produced by high performance liquid chromatography. 55

Figure 21: Calibration curves for glyoxylic acid. A: Logarithmic calibration curve showing detection threshold line. The red line represents the approximate threshold of detection by the HPLC apparatus (at a signal of 1.2×10^7). The black line bisects the points of the calibration curve and represents an R^2 value of 0.96. B: Calibration curve showing linear regression..... 64

Figure 22: Weight loss of PDSII and silk sutures over 91 days. (Black error bars represent standard error from the mean). 68

Figure 23: The percentage weight loss of PDO patch and a PDSII suture over 91 days. (Black error bars represent standard error from the mean)..... 69

Figure 24: Change in the pH of the PBS incubation solution containing 20mg PDO patch over 47 days. (Black error bars represent standard error from the mean). 70

Figure 25: HPLC chromatograms for glyoxylic acid (A), glycolic acid (B), lactic acid (C), and the polydioxanone degradation product (C). Note each peak is given a corresponding time in minutes e.g. 5.058. In the table below each graph, each peak time corresponds to an area under the curve, which correlates with the concentration of the detected compound. The 4 graphs demonstrate that all 4 compounds generated 2 peaks at very similar time points: approximately 3.5 and 3.9 minutes. 71

Figure 26: The mean chromatographic peaks of three monomers (GLA: glycolic acid, GOX: glyoxylic acid, LA: lactic acid) and the degradation product of PDO (all concentrations were 20mg/ml). (Black error bars represent standard error from the mean)..... 72

Figure 27: The chromatographic signal generation of polydioxanone solutions after different lengths of hydrolysis in NaOH. (Black error bars represent standard deviation from the mean)..... 73

Figure 28: Cumulative HPLC signal generated from the filtrate (in terms of areas under the peak). The straight red line represents the threshold of detection. This demonstrates that none of the filtrates reach the threshold of detection. 74

Figure 29: Cumulative HPLC signal generated from the retentate (in terms of areas under the peak). The straight line represents the position of the threshold of detection. Unlike Figure 28, here the concentrations of monomer gained from the retentate breach the threshold of detection. 75

Abbreviations

BMP	Bone morphogenic protein
CO_2	Carbon dioxide
DAPI	4',6-diamidino-2-phenylindole (a fluorescent stain)
DLPLG	Poly(D,L-lactide-co-glycolide)
ESEM	Environmental scanning electron microscope
GLA	Glycolic acid
GOX	Glyoxylic acid
HCl	Hydrochloric acid
HFP	Organic solvent 111,333,hexafluoro-2-propanol
HPLC	High performance liquid chromatography
LA	Lactic acid
MSC	Mesenchymal stem cell
NaOH	Sodium hydroxide
PBS	Phosphate buffered solution
PDO	Polydioxanone
PDSII	Commercial name of polydioxanone suture material
PGA	Polyglycolic acid
PGLA-910	90/10 glycolide/L-lactide copolymer
PLA	Polylactic acid
PLGA	Poly-lactic-glycolic acid
PLLA	Polylactic acid
PPDx	Polydioxanone as referred to by Sabino *et al*

1 Introduction

1.1 Background

1.1.1 Anatomy and pathology

The rotator cuff is a group of four muscles and their tendons that stabilise the shoulder joint by forming a musculotendinous cuff around the glenohumeral joint. These muscles originate from the scapula and insert into the humerus. Their functions are to contribute to movements at the joint and to maintain the stability of the joint. The shoulder joint is a multiaxial synovial ball and socket joint with more planes of movement than any other joint in the body – flexion, extension, abduction, adduction, lateral and medial rotation are all possible – yet the freedom to perform these movements necessitates a potential instability that renders the joint susceptible to dislocation.

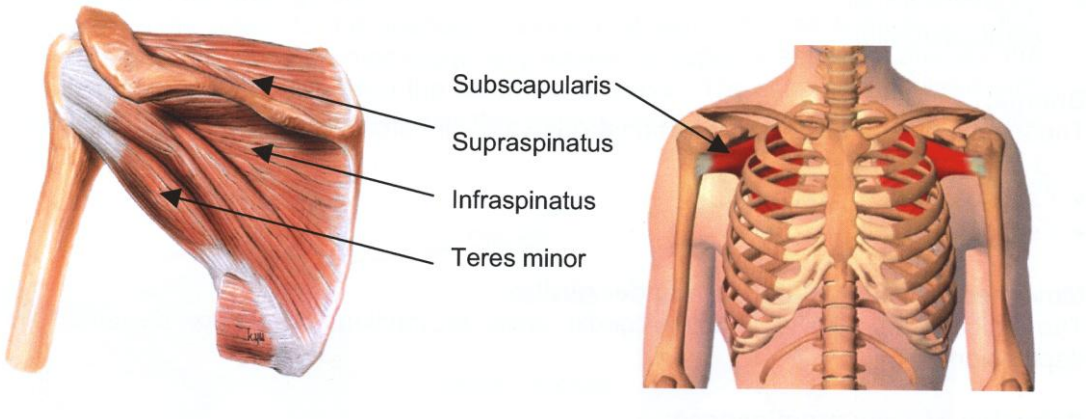


Figure 1: The muscles of the rotator cuff viewed from posterior (left) and anterior (right). Image courtesy of www.wordpress.com.

Tears of the rotator cuff are common, causing disabling pain, weakness and loss of motion. Initial treatment is often conservative but surgical repair may be indicated if

non-operative management fails. Examples of surgical repair include open surgical tendon repair with anterior acromioplasty, and arthroscopic debridement with subacromial decompression. Failure rates of rotator cuff repairs can be as high as 90% due to poor healing capacity of the involved tissues (1), and excessive tension at the repair site causing the suture to cut through tendon (2). There is therefore a subsequent need for novel strategies for repair which address these issues.

1.1.2 Tendon repair implants

The high failure rate of tendon repairs has led to extensive research into potential implants to enhance surgical attachment, giving rise to a series of generations of implants. Rotator cuff implant development can be described in terms of 3 generations of rotator cuff repairs.

1. The first generation has comprised standard suture fixation with either absorbable or non-absorbable sutures, depending on the pathology (Figure 2A).

2. The second generation has used an augmentation device providing a tendon-bone bridge and scaffold for host tissue deposition and in-growth. It comprises a slowly degrading and biocompatible polymer such as poly-L-lactide that can be used for irreparable tears, and to reinforce suture repair lines (3).

3. The third generation has used natural collagen-rich extracellular matrix scaffolds. Some are derived from human de-cellularised allograft skin, leaving a matrix containing elastin, collagen and proteoglycans. An example is Graft Jacket (Wright Medical) as seen in Figure 2B. Others originate from foetal bovine dermis (4).


A


B

Figure 2: Common methods of rotator cuff repairs such as standard double row suture fixation of sheep rotator cuff using non-degradeable Fibrewire sutures (A, O. Hakimi et al 2012, unpublished) and GraftJacket (B, Wright Medical) a de-cellularised skin matrix, thought to promote tissue growth (5).

1.1.3 A fourth generation of rotator cuff repair?

This research group proposes a fourth generation implant that does not necessarily have any mechanical advantage to the tendon-bone bridge, but instead provides biological enhancement to the standard orthopaedic fixation. Platelet-rich plasma injections, for example, are used in the treatment of tendon injuries by promoting healing while simultaneously facilitating the release of the body's natural growth factors (6).

This thesis will focus on studying a novel implant which belongs to this recent generation of rotator cuff therapies. Electrospun from polydioxanone (PDO), this implant will allow the injection and subsequent slow release of agents that will enhance the tendon's natural healing processes. The implant is in the form of a patch whose qualities include swift degradation, minimal tissue reaction, and the ability to retain cells and fluids within its matrix (7). For example, protein-rich plasma, stem cells, or other agents beneficial to wound healing will be injected into the patch post-operatively. Within 4-6 weeks, as the PDO structure degrades, the incorporated cells

would be released directly onto the damaged tendon. This would provide a local and timed release delivery system which would then be fully degraded and excreted. The hypothesised advantage is that the injected agents will not immediately disperse, but will be localised and contained directly above the repair.

This thesis will specifically examine the degradation of polydioxanone. It will establish the time frames in which different structures of PDO degrade, and what properties the degradation products possess. For instance, when using tenoblasts on the PDO platform, it is of interest to study the effect of the change in pH that may results from the degradation. The morphology of the material as it degrades is also of interest since not only will this affect the timings of degradation, but also the concentrations of different breakdown products.

1.2 Polydioxanone as a biomaterial

This section will briefly describe polydioxanone and its properties with particular reference to their relevance for the application outlined above.

1.2.1 Polymers

A polymer is a macromolecule derived from repeating monomers typically connected by covalent bonds. Polymerisation is the process of connecting the monomers to form the polymer. During the polymerisation process, chemical groups are lost from each monomer, leaving the repeating unit. Biodegradable polymers are either synthetic or natural. Synthetic polymers such as PDO and PLLA (polylactic acid) are advantageous since they have more uniformity of production when compared to natural polymers. They are also free of the immunogenicity which can blight the use of tendon allografts

(8) since they degrade into small acidic products that generally do not invoke immune responses. They can also be tailored to provide a wider range of properties (9).

1.2.2 Polydioxanone

Polydioxanone (PDO) is an absorbable polymer from the α-hydroxy acid polymer family, and used as a surgical suture for a range of soft-tissue approximations. It was first developed in 1981 and is a colourless, crystalline, bioabsorbable synthetic polymer (10). An inert purple dye is added during the manufacturing process of the suture to provide a purple hue for handling purposes (11). The commercial name of the polymer suture material is PDSII (Ethicon, USA). During the formation of PDO, as shown schematically in Figure 3, the monomer is in a ring structure known as paradioxanone. Ring-opening polymerisation with heat and an organometallic catalyst results in poly(ether-ester) formation (12).

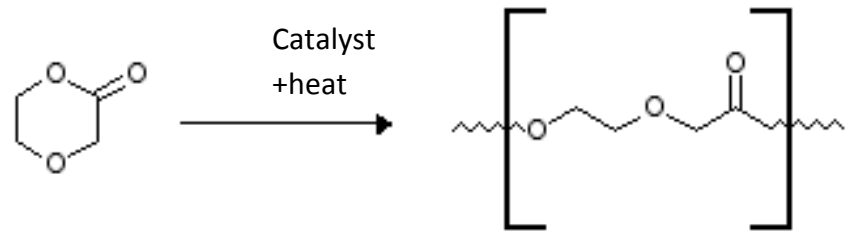


Figure 3: The formation of the polydioxanone polymer from the p-dioxanone monomer.

The ideal polymer for a biomaterial application must not evoke an unwanted tissue response disproportionate to its beneficial effect. It must be metabolised after performing its purpose and leave no trace, be easy to manufacture and have an acceptable shelf life. It must also be easily sterilised to allow *in vivo* use(9). PDO

conforms to all these requirements and thus presents an example of an ideal material for this application.

1.2.3 Synthesis

The PDO patches used in this study were formed by the process of electrospinning, schematically shown in Figure 4. This is a polymer processing technique that utilises an electric field to form fibres from a polymer solution (PDO in the organic solvent 111,333,hexafluoro-2-propanol (HFP)). It allows the production of nanofibrous, non-woven structures (10) that can act as a scaffold.

Electrospinning involves a solution of PDO in the organic solvent HFP being dispensed from a syringe onto a target (Figure 4). An electric current is passed through the syringe needle onto a designed target (sometimes rotating). The rotations per minute can be adjusted to create randomly arranged fibres or aligned fibres (10) in the form of mats. These can then be cut into the desired size. Boland *et al* found a strong linear relationship between the concentrations of PDO in solution and the diameter of the fibres produced (10).

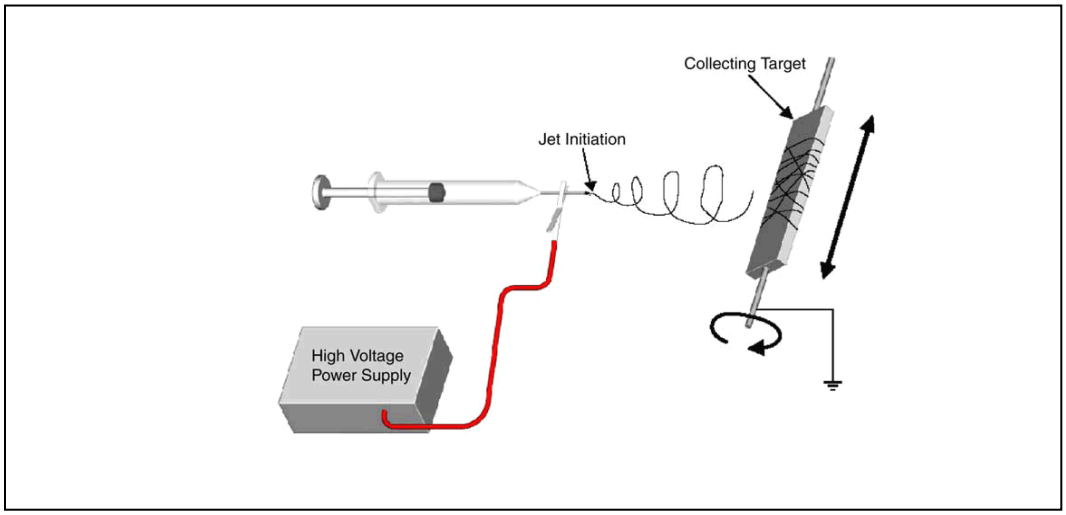


Figure 4: Schematic of electrospinning apparatus. Boland et al (10)

1.2.4 Properties

Polydioxanone has a crystalline fraction of 55%. Percentage crystallinity represents the degree of structural order in a solid, and has a large influence on the diffusion, transparency, hardness and density of a material. Typically, the polymer chains are composed of both crystalline and amorphous regions. The amorphous regions are generally disordered, but have some structural order over short distances. The higher the crystalline fraction, the stronger the construct, due to more order and less slippage between adjacent chains. This slippage is time dependent under load, conferring a viscoelastic property to the material (13).

Temperature has a profound effect on polymers. Polydioxanone has a "softening temperature" or glass-transition temperature of between -10^0C and 0^0C. Glass transition temperature is the temperature range within which a glass-forming liquid transforms into glass during rapid cooling. Below this temperature the material is hard and stiff, while above it the material becomes soft and rubbery. Consequently, for bioabsorbable polymers, it is essential that they have a glass-transition temperature below body temperature (14). This is because a material will be more ductile at these temperatures.

1.2.5 Degradation

Generally it is desirable for an implant to disappear once the healing is complete, as a slower degrading implant may be a source of infection and continuous inflammation. α- hydroxy acid polymers are synthetic polymers designed to degrade by hydrolysis. They have hydrolytically unstable backbone linkages, usually ester bonds. Degradation

of these polymers occurs through a non-specific scission of these ester bonds. PDO is either metabolised to glyoxylate and excreted through the kidneys, or is converted into glycine and then carbon dioxide and water (13). A schematic representation of the degradation appears in Figure 4.

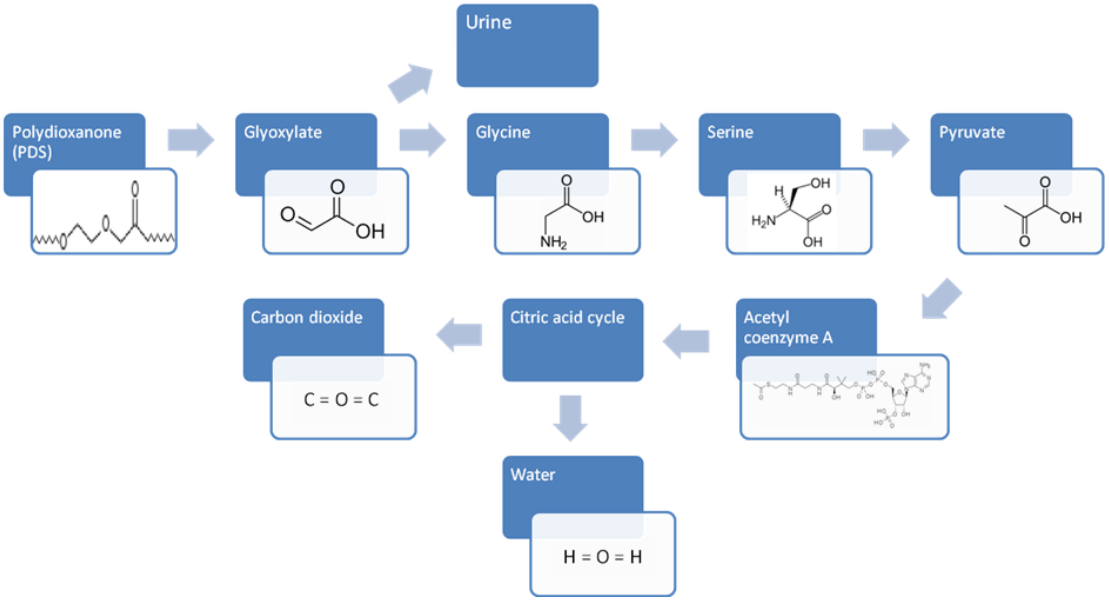


Figure 5: The excretion of polydioxanone (11).

This process of degradation depends on PDO's porosity, crystallinity, and molecular weight (13). The factors which accelerate polymer degradation are summarised by Middleton *et al* (9) as follows:

- Monomer hydrophilicity - a more hydrophilic monomer will encourages the hydrolytic degradation of the polymer.
- Polymer extremity (end-group) hydrophilicity and acidity.
- Hydrolytic group in the middle structure or 'backbone' of the polymer.
- Ratio of crystallinity to amorphous regions - less crystallinity and a higher proportion of amorphous regions results in kinetically favoured hydrolysis of these amorphous regions (15).

- Device size - smaller implants have reduced degradation times.
- Surface area to volume ratio - higher surface area exposes more hydrophilic groups to the solvent, thus accelerating degradation.

The ability to tailor degradation rates of polymers broadens the appeal of biodegradable polymers as an orthopaedic implant since they could be custom made depending on the pathology present. For instance, water uptake and degradation rate can be accelerated with the replacement of ester end groups with carboxylic acid end groups on poly(D,L-lactide-co-glycolide) (DLPLG) polymers (similar in structure to PDO). The acidic end-groups increase the hydrophilicity and catalyse degradation (16).

The hydrolysis that takes place during polymer degradation occurs in two stages. Primarily, water penetrates the bulk of the device, preferentially attacking the ester bonds in the in the amorphous region of the structure and dividing long polymer chains into shorter fragments. This first phase is the reason why there is an initial reduction in molecular weight without any loss in macrostructural properties, since the implant matrix is still held together by the crystalline regions (9). Subsequent loss of physical properties occurs as water enters and fragments the structure. The second phase often involves enzymatic attack of the fragments, resulting in rapid polymer mass loss (14).

Hydrolysis of PDO by scission of the long polymer chains begins immediately on implantation and occurs in acidic or basic conditions. Water enters the structure via pores in its surface. Consequently, porosity and surface area are implicit in the degradation rate (13). The stages of PDO degradation are described in chapter 4.2.3.

Perhaps counter-intuitively, materials that are less porous have been shown to retain the acidic breakdown products (CO_2) within their structure, causing an acceleration of the hydrolysis (17). Similarly, an acidic local environment such as that found during infection or an inflammatory reaction may also accelerate the degradation, and in doing so, further acidify the locality thus causing a 'snowball' effect.

1.2.6 Tissue response

As previously mentioned, it is important that an implant doesn't invoke a strong foreign body inflammatory response or leach toxic particles. This is because a severe or lengthy inflammatory response to an implanted material could hamper the inflammatory phase of wound healing and subsequently reduce the strength of the repair (18). In this regard it is essential that the locality in which the implant is situated is able to disperse the material's degradation products (in the case of PDO, acid), otherwise an inflammatory response with cell necrosis and apoptosis may occur (19). There have been a number of publications looking at tissue response to PDO. Middleton *et al* found PDO to be free of immunogenicity with minimal inflammatory response. In contrast, Metz *et al* investigated rabbit tissue response to PDSII sutures *in vivo*. They found that, initially, the suture became covered with a fibrous tissue, with infiltration of inflammatory cells peaking at 4 days post-implantation. The inflammatory cell density subsequently declined sharply for a week, and then more gradually. The composition of the inflammatory infiltrate was initially both acute and chronic inflammatory cells, but macrophages and histiocytes dominated 1 week post-implantation. As the inflammatory cells dissipated, fibroblasts were recruited to the wound, resulting in remodelling of a collagen matrix. The inflammatory reaction to

PDSII was 2.5 times greater than that to the Prolene suture (non-absorbable) (20). Kalfa *et al* used electrospun bioabsorbable PDO patches seeded with mesenchymal stem cells (MSCs) in the right ventricular outflow tract of growing lambs. They found a reduced inflammatory response compared to polyglycolic acid (PGA) and polylactic acid (PLA), as well as cells derived from the graft in the tissue once the patch had fully degraded (21). Further research in this area is required.

1.3 Cell recruitment and attachment

Cell migration, division and differentiation depend in part on cell adhesion (22). The initial attachment of cells to an implant therefore has a significant influence on the subsequent tissue response to the implant. Sabino *et al* have compared PDO (referred to by them as PPDX) to other biodegradable polymers such as PGLA-910 (a co-polymer of 90% Glycolide and 10% L-lactide used as a synthetic absorbable surgical suture). They found that PDO has conferred a favourable support to fibroblasts and slowly degrades leaving no cytotoxicity. These are essential qualities for a biodegradable implant (23).

Although the suggested role of the PDO implant studied here is that of a platform for extrinsic administration of cells (such as stem cells), if the implant itself can cause the migration of desirable intrinsic cells then this would be advantageous. Baumann *et al* observed osteoconductive properties of PDO sheets when used in *in vivo* animal studies. Unfortunately that has not been observed in the human patient group (24). However, the potential for synergistic intrinsic and extrinsic cell attachment is interesting. Kontio *et al* looked at the foreign body reaction, and capsule formation

around two bioresorbable implants. They performed histology on PDO implants and found that the histology of the peri-implant capsule exhibited an inner zone rich in cells, and an outer zone of connective tissue around both materials(25).This raises the interesting possibility of the capsule inhibiting interaction of the implant with the surrounding tissue.

1.3.1 Mechanical properties

An implant in the rotator cuff will be subject to a high degree of mechanical stresses, therefore it is important to understand how different materials react to these conditions. A larger surface area of a biodegradable implant confers greater scope for hydrolysis, as do high levels of mechanical stress. The latter is due to microstructural cracks which appear throughout the outer exterior as degradation begins to occur and increases the surface area, as well as reducing macro structural mechanical strength (13). Polydioxanone sutures (commercially known as PDSII) have been found to degrade over approximately 60 days with a complete loss of mass over 9 to 12 months (13). As a surgical suture, PDO has been demonstrated to have higher flexibility and strength retention, lower inflammatory response rates, and slower absorption rates when compared to Vicryl and Dexon sutures(11). 50% of the breaking strength of the monofilament suture is lost after 3 weeks, and 100% is lost after 6 months. This time scale is beneficial for slow healing wounds such as those found in rotator cuff tears.

The disadvantages of polydioxanone as a suture include its high shape memory which makes it more difficult to manipulate and control in surgical situations, and low surface friction which means knot loosening is commonplace, and knot retention is difficult. However, coupled with polydioxanone’s biocompatibility, flexibility, and degradation

rate, these properties make the material potentially suitable for uses in tissue engineering (10).

1.4 Potential for tissue engineering and Orthopaedic applications

As an orthopaedic implant, biodegradation is desirable since it does not necessitate a second surgical event for extraction of the implant as with permanent metal implants (9). PDO has already been used clinically in orthopaedic plates, pins and screws for fracture fixation (26). However, drug delivery provides another exciting potential role for PDO (9), and recent work in our lab focused on the use of PDO as a degradable scaffolding structure that can be injected with biologically active factors or cells. A variety of cells and biologically active factors are being postulated as suitable for injection into the PDO host. These may include stem cells, antioxidants and growth factors. For example, bone morphogenic protein (BMP) has been used by Wang *et al* to induce cartilage and bone formation, yet they have concluded that BMP delivery requires a suitable delivery system (27). In another study, PLGA (poly-lactic-glycolic acid), a similar polymer to PDO, has been used as an implant to release ciprofloxacin-containing microcapsules. This method has the potential for use in the treatment of osteomyelitis (28). Stem cells have stimulated great interest in orthopaedics and bone tissue engineering (29), however, an efficient mechanism to ensure local effects and prevent widespread dispersion of the cells is yet to be refined.

1.5 Scope of study

The aim of this thesis is to investigate and characterise the degradation of PDO scaffold patches. Degradation in this context refers to the process of simplifying or breaking down a molecule into smaller parts. In the case of the PDO patch, the hypothesis is

that the bulk of the patch will lose weight as bonds within the polymer are broken and molecules are degraded away from it. Weight loss is therefore investigated. pH is also used as a marker of hydrolysis of PDO since the process produces hydrogen ions. Not only will quantifying pH change demonstrate the dynamics of PDO degradation, but it will also provide useful information regarding the acidity of the environment that the PDO patch and any attached cells will be exposed to. In this way, the mechanisms of degradation of PDO will be investigated. The morphology of the degradation will also be assessed using imaging techniques to demonstrate the macrostructure of PDO under magnification and how this may change over time. The addition of cells to the PDO patch will also provide an interesting further dimension to the morphological observations. Attempts will also be made to identify the degradation product and mechanism of degradation using high performance liquid chromatography (HPLC).

The experiments presented in this thesis were performed *in vitro,* but were aimed at contributing to the understanding of how the patch will perform as a biodegradable implant *in vivo*.

2 Characterisation of novel PDO patches by electron and fluorescent microscopy

2.1 Introduction

As discussed earlier, it is still necessary to build up an understanding of the alteration in morphology as well as the rate and timing of the degradation of electrospun PDO scaffolds. Thus, the aim of the study presented in this chapter was to provide detailed images of the material as it underwent degradation and build up an understanding of the alteration in morphology, as well as the rate and timing of these alterations.

Scanning electron microscopy is a technique which enables the imaging of a sample by scanning it with a beam of high-energy electrons in a rectangular pattern of image capture (raster scan pattern). Signals are produced when these electrons interact with the atoms on the surface of the sample. These signals contain information on the topography composition and electrical conductivity of the sample. A wide range of magnifications are possible, from 10x to 500,000x.

Environmental Scanning Electron Microscopy (ESEM) provides the opportunity to image insulating (i.e. non-conductive) materials in a hydrated state without the conductive coating used in standard electron microscopy (30). Unlike conventional electron microscopy, where a high vacuum is maintained, ESEM makes use of a multiple aperture graduated vacuum system. This allows specimens to be imaged under water vapour, nitrogen, or nitrous oxide (31). As a results, the ESEM chamber can be maintained at low pressures between 1 Torr and 10 Torr, while the column and gun remain at pressures of approximately 7.5×10^{-7} Torr (32). In addition, by controlling

the temperature of the specimen using a Peltierstage, and by using the correct pump-down procedure, dehydration of wet samples can be inhibited (33). Samples can therefore be viewed in their natural, hydrated form.

The electrons emitted from a specimen in the ESEM, whether secondary or higher energy backscattered electrons, have to move to the detector through the gas-containing chamber and consequently undergo collisions with gas molecules. In this way, a cascade amplification process occurs resulting in far more electrons being detected than were originally emitted from the sample (34). The positive ions that are formed drift back to the surface of the specimen, whereupon they neutralize the charge build-up associated with electron microscopy of insulating materials. For this reason, insulators can be viewed in ESEM without the need for a conducting coating.

Since the scaffolds investigated here will be in a hydrated state in vivo, its visualisation in an ESEM would be more relevant then in dehydrated form (SEM). Moreover, specimen preparation for ESEM is faster and simpler, and the specimen surface is un-modified by either the chamber vacuum or the sample gold-coating common to SEM.

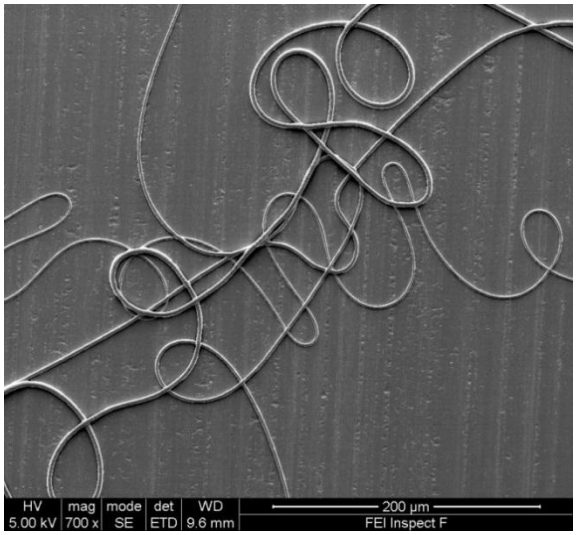
In this study, specimens of electrospun PDO in various stages of degradation were viewed in an environmental scanning electron microscope. Later, fluorescence microscopy was used to visualise samples with tenoblast cells incorporated into them. The images allowed a visualisation of the attachment of cells to the electrospun fibres as well as an observation of the density of cells and their distribution across the material. In parallel, the extent of the degradation of the patch at different time points was recorded in order to link the morphological phenomena with the different stages

of degradation. Using these microscopy techniques, it was possible to describe changes to the morphology of PDO as it degraded.

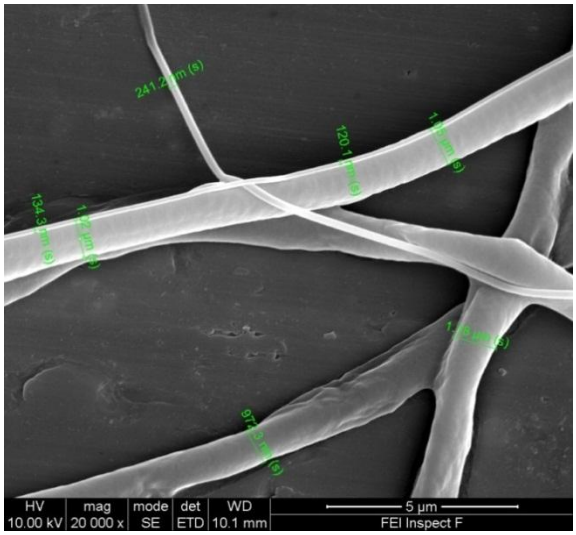
2.2 Materials and Methods

2.2.1 Electrospinning of the polydioxanone patch prototype

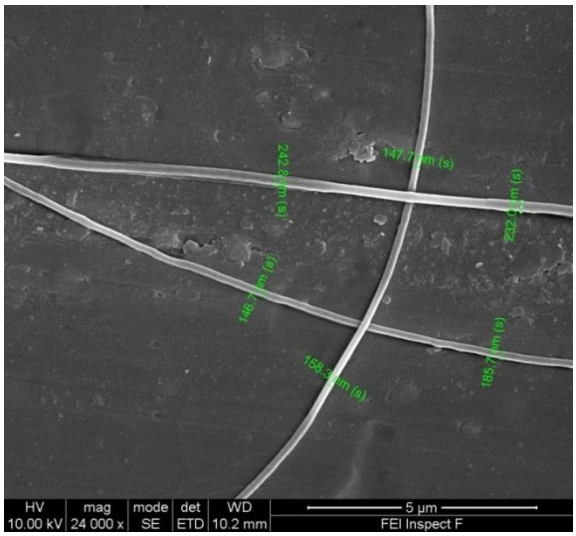
Electrospinning was performed by Dr. Urszula Stacewitz at Nanoforce Technology, London, UK. Briefly, poly(dioxanone) (Sigma-Aldrich, U.K.) was dissolved in 1,1,1,3,3,3-Hexafluoro-2-propanol (HFP, Fluka Analytical, U.K.) to produce a polymer concentration of 7% weight-by-volume in solution. Fibres of PDO were electrospun from a single nozzle with a distance of 26.5 cm between the nozzle and grounded electrode, and a voltage of 13.5 kV. The polymer solution was then ejected from a syringe pump at a flow rate of 1 ml/h. The voltage applied at the metal needle caused a charge build-up at the meniscus of polymer solution hanging from the end of the nozzle, until cone-jet formation occurred and stretching jets projected towards the ground electrode, and solid nanofibers were deposited on aluminium foil. Approximately 10 cm^2 patch was produced in 4.5 hours. To remove thinner sections of the electrospun patches, the sample was bathed in 70% ethanol and scraped gently from the aluminium foil with forceps. Thicker areas of the patch could easily be peeled from the foil. The electrospun PDO fibre diameter, measured using scanning electron microscopy (Inspect F, FEI Company, U.S.A./E.U.), was between 0.1 and 1μm, as demonstrated in Figure 5. The density of electrospun patches was measured using a gas pycnometer (AccuPyc 1330 He, U.S.A.).



A



B



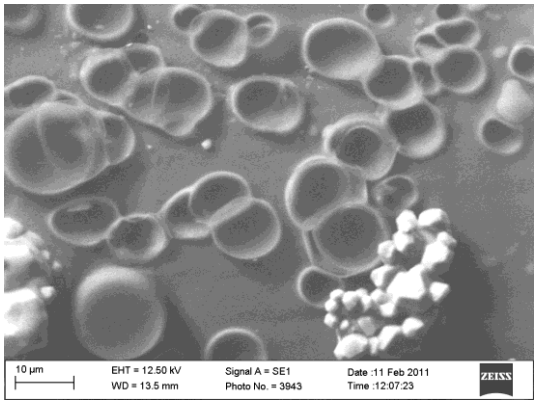
C

Figure 6: Electron micrographs showing randomly oriented electrospun polydioxanone fibres (A) and the variation in fibre diameter (B,C). Images courtesy of Dr. Urszula Stacewitz.

2.2.2 Environmental Scanning Electron Microscopy

The environmental scanning electron microscope used was a Carl Zeiss Evo LS15 variable pressure scanning electron microscope, equipped with a LaB6 source and a range of detectors for electron imaging. A number of different samples were viewed in the ESEM. Dry electrospun PDO patches were visualised to demonstrate the original structure of PDO pre-degradation. PBS-incubated electrospun PDO patches in various stages of degradation allowed us to describe the macro-processes that occur leading to loss of mass of the material. Electrospun PDO patches seeded with tenoblasts were also viewed. This was to demonstrate the structural interactions between cells and polymer, and to enable observation of the spread of cells through the polymer layers.

It was necessary to perform some optimisation of the image acquisition, as the high vacuum and the constant beam of electrons could modify the surface of the samples. This resulted in bubbling on the surface of samples (Figure 7). Thus, for high magnifications PDO samples were gold coated using a gold-sputter (Bio-Rad SEM Coating System with gold targets supplied by Agar Scientific Ltd, England). This didn't affect the quality of the images but prevented the visible damage to the samples seen in Figure 7.

A 

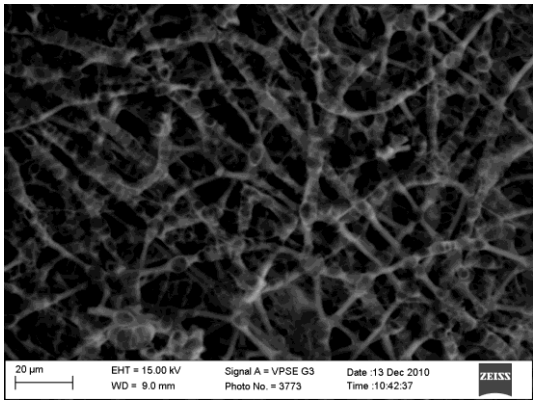
B 

Figure 7: 'Bubbling' on the surface of (A) a PDSII suture and (B) a PDO electrospun patch. Note the crystals of salt visible in image A.

Samples were initially viewed uncoated at magnifications in the range of x500 and x1000. The gold sputter device was then used to coat additional samples, which could be viewed at a higher vacuum and therefore at higher magnifications (up to 5,000x).

A tensile testing machine equipped with a 22N load cell (Bose Electroforce, Eden Prairie, USA-MN) was used to stretch a patch before viewing it in the ESEM. The aim of this was to get images of a patch that has undergone tensile stress such as may occur *in vivo* when the patch is sutured within the rotator cuff.

2.2.3 Fluorescence microscopy

Electrospun PDO patches that had been incorporated with primary tenoblasts, as well as those which hadn't, were stained using the following protocol. Briefly, cells explanted as previously described were received at passage 2 from Dr. Osnat Hakimi. Cells were seeded on 0.5cm^2 patch segments at a concentration of 10^5 cells per patch and grown under sterile conditions. After between 7 and 30 days in culture, the patches were fixed in 10% formalin for 5 minutes before being washed 3 times in PBS for 2 minutes. They were then incubated in 0.1% Triton X-100 (in PBS) for 5 minutes

before being washed again in PBS for 2 minutes. DAPI (1/500) and Actin-phalloidin (1/40) were then diluted with PBS in the same tube: 1µl DAPI with 1ml PBS in 1 tube, and 12.5µl Actin-phalloidin with 12.5µl PBS in 1 tube. A 50µl aliquot per coverslip was applied and the samples were then incubated for 30 minutes in the dark before being washed once again in PBS for 2 minutes. There was one final washing in MilliQ water to complete the protocol. The samples were then viewed using fluorescent microscopy (BX40, Olympus or eclipse TE300, Nikon) with either the DAPI or actin-phylloidin stain highlighted. The images were then merged.

2.3 Results

2.3.1 ESEM

As can be seen in Figure 9 A to E, the fresh electrospun PDO patches appeared to have many long, unbroken fibres that spanned the width of the images. They formed layers that could be seen to intertwine to some extent though in the main were planar. The arrows on Figure 8 highlight a single long fibre that takes a curved course across the image. Figure 9B shows a patch that was stretched using the tensile testing machine. Figure 9C-E uses a high magnification to show the layered nature of the fibres as they intertwine within the patch.

Figure 10A to G shows the appearance of the PDO patches after 30 to 56 days incubation in PBS. Two investigators concurred that their macrostructure was maintained to a high degree on observation through the microscope. The gross structure and dimensions of the patch were retained. Figure 10A shows a patch after 30 days degradation demonstrating surface erosion of superficial fibres, with deeper fibres maintaining their length. Figure 10B-G show PDO patches after 56 days

degradation. There are no long, unbroken fibres but rather short, chopped fragments. Overall, despite the lengthy degradation period, patches were still grossly intact.

Figure 11A-G are ESEM images of electrospun PDO patches that have been seeded with tenoblasts and incubated for 42 days. The cells can clearly be seen spread between the fibres of PDO in a regular manner. It is also apparent, on observation, that the cells have penetrated into the structure beyond the superficial layer with some cells only just visible due to fibres overlying them. This suggests that there is a higher concentration of cells than that merely on the surface such as seen in Figure 11B. Instead, cells appear to be spread throughout the thickness of the patch. This is further demonstrated in the fluorescent microscopy images in Figure 13 and Figure 14.

Although these images do not project the 3D nature of the patch or the depth of cell penetration into it, observation by eye provided the depth perception that confirmed cells present within and throughout the patch. Figure 11C, D and H shows examples of how fragments that had broken away from the main body of the patch had cells attached to them. These were pieces that fell off the patch during incubation and were fixed to a slide for ESEM viewing.

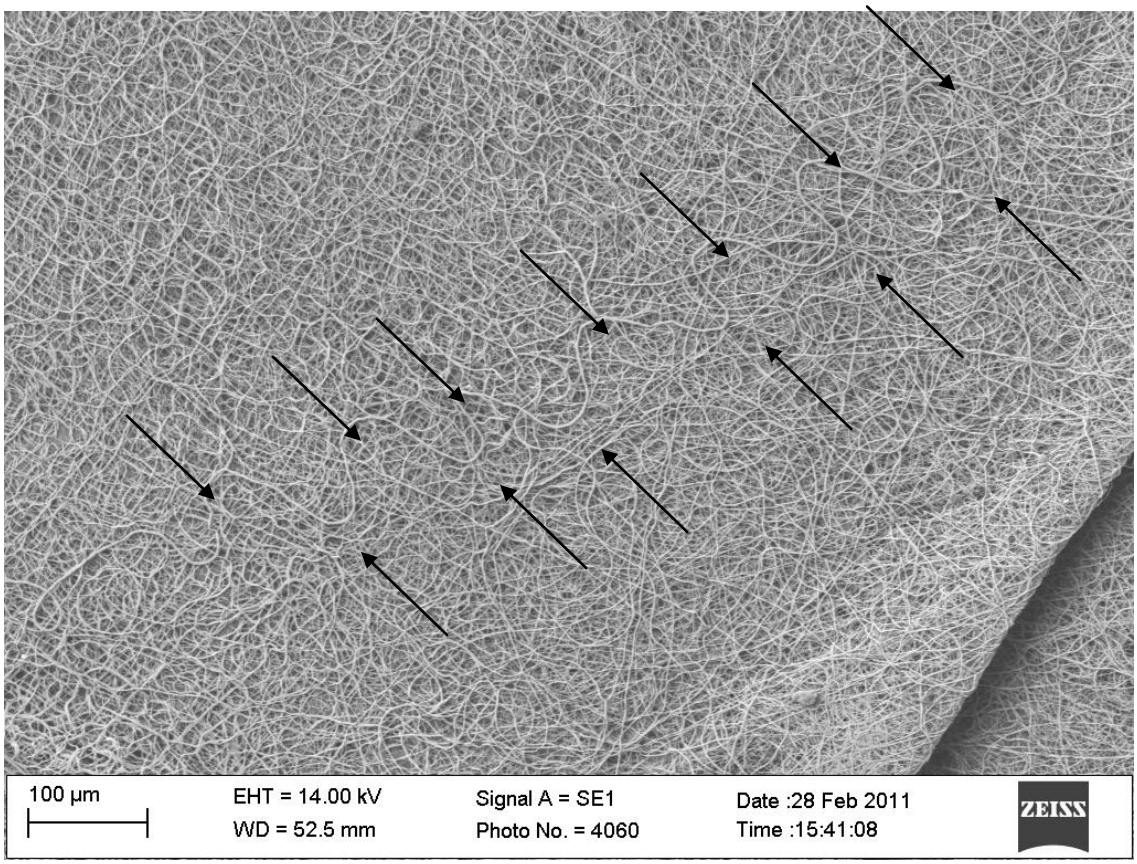
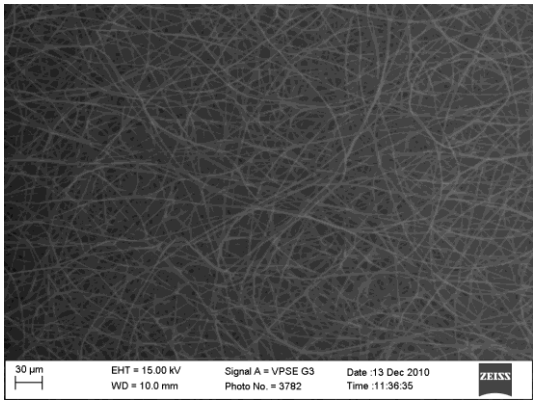
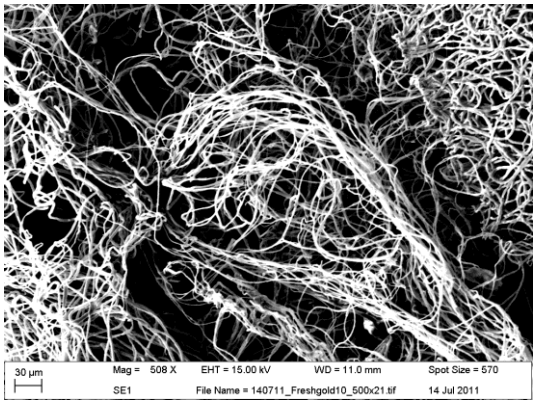


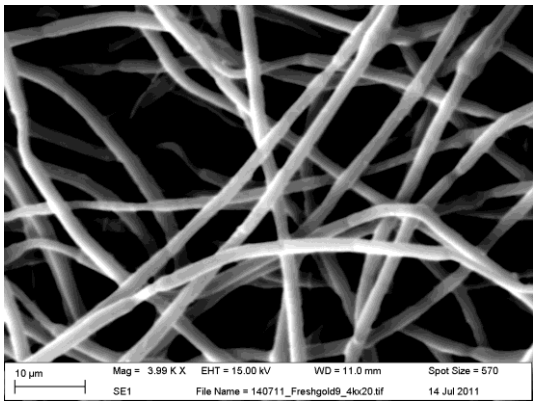
Figure 8: An un-degraded, gold-sputtered polydioxanone patch viewed in an ESEM. Of note are the long, continuous fibres that stretch across the patch (one in particular highlighted by black arrows.



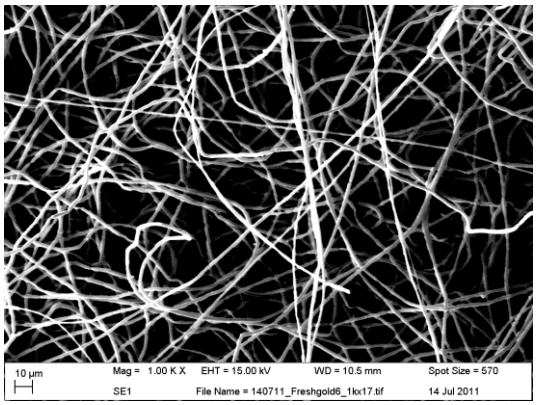
A



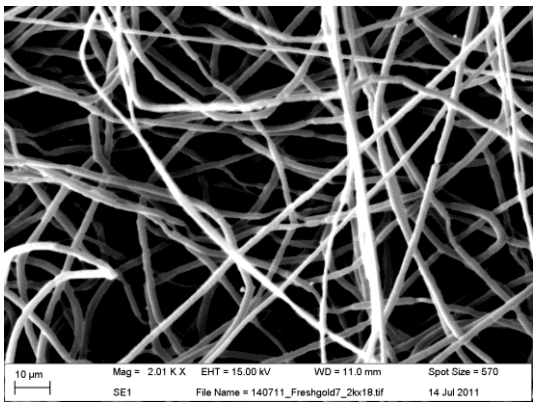
B



C

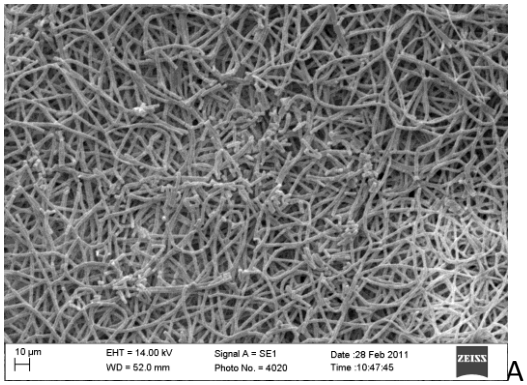


D

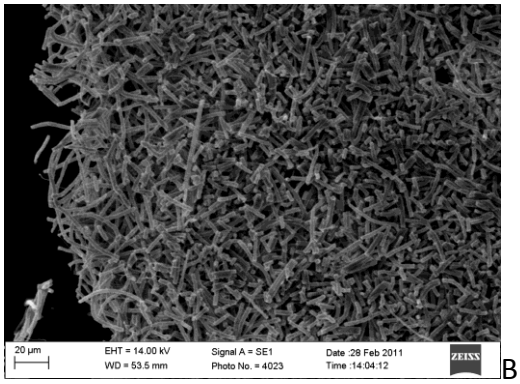


E

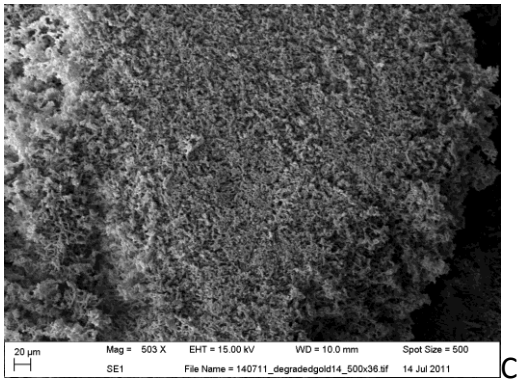
Figure 9: ESEM images of fresh electrospun PDO patches. A, B, C, D and E show long continuous fibres running across the patches prior to degradation. Image B shows an undegraded PDO patch at 500x. This patch has had tensile stress exerted on it which manifests in less regular layering of fibres. All these samples were gold-sputtered.



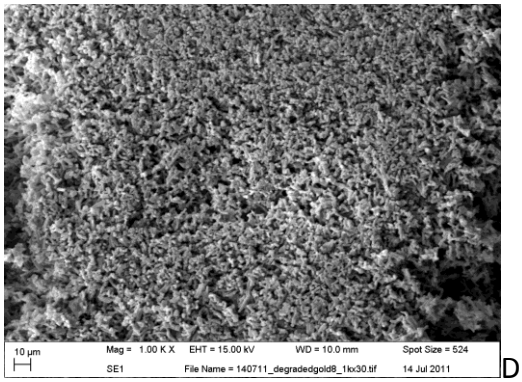
A



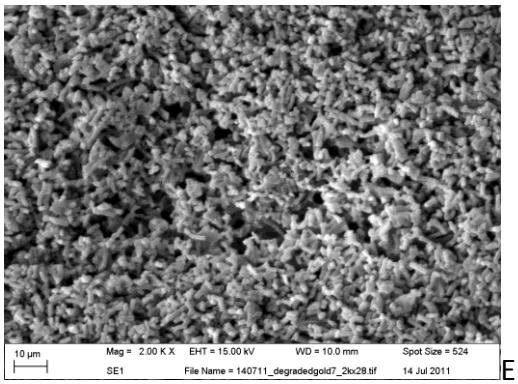
B



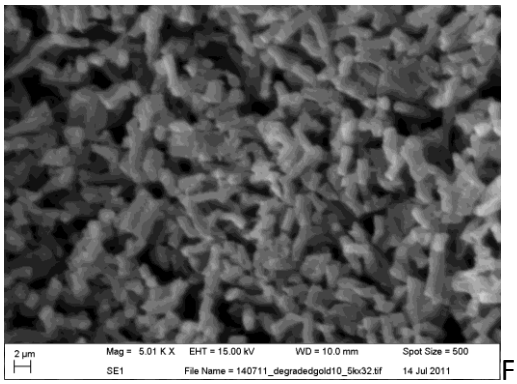
C



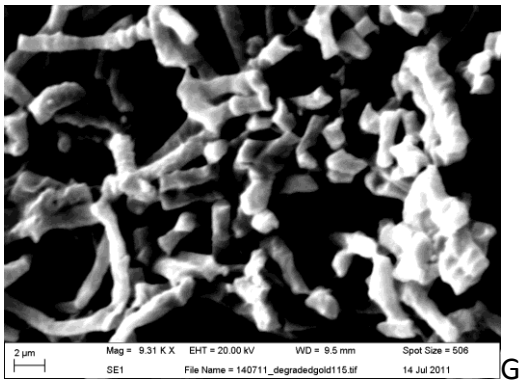
D



E



F



G

Figure 10: ESEM images of electrospun PDO patches degraded in PBS for 30 days (A) or 56 days (B to G). Note the short chopped nature of the polymer fibres. After 30 days (A) surface erosion of the fibres has occurred, while after 56 days (B to G), deep and thorough degradation has affected all visible fibres.

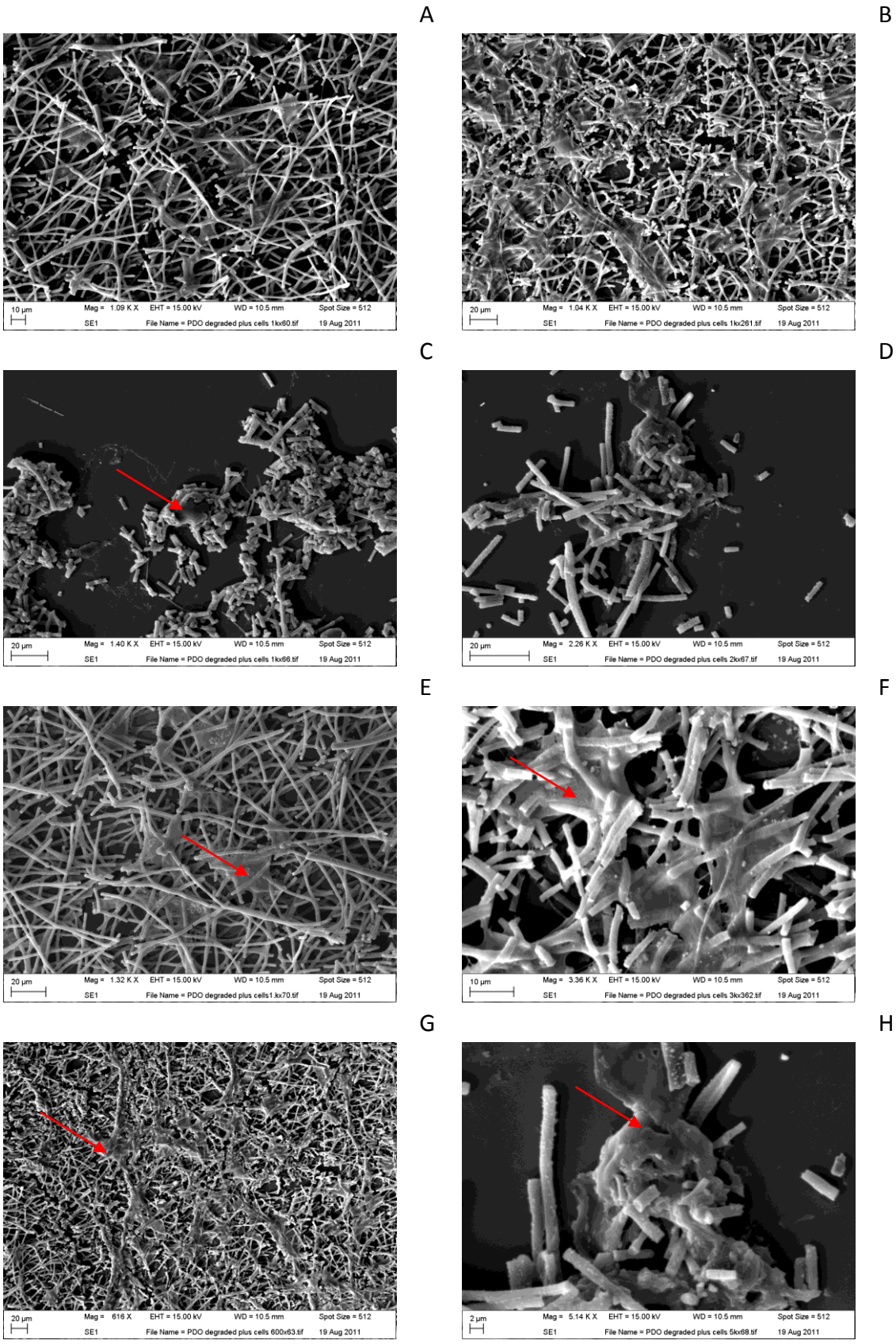
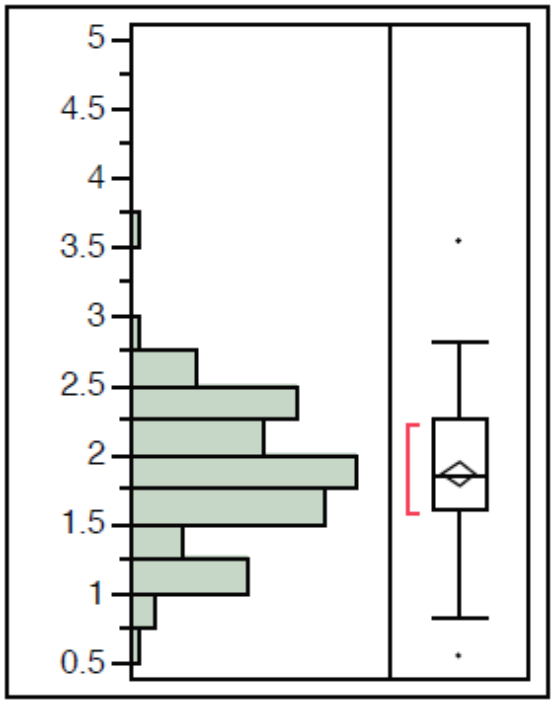
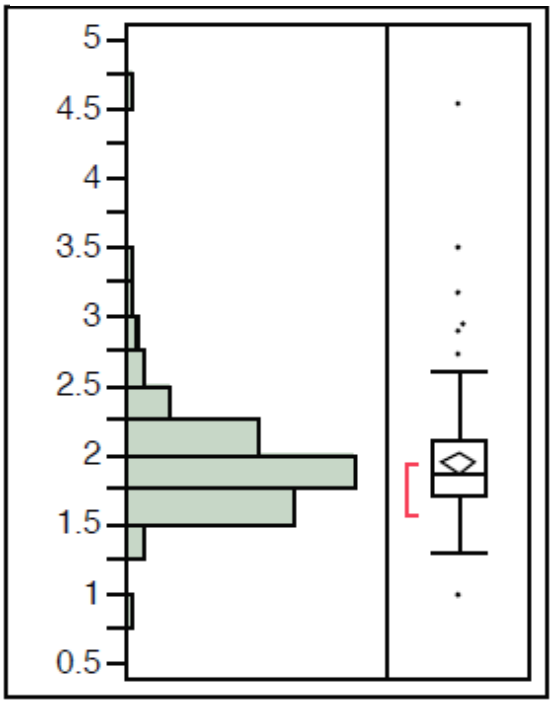


Figure 11: ESEM images of electrospun PDO patches that have been seeded with tenoblasts and incubated for 42 days, showing the patch (E, F, G) as well as fragments which were seen around it (C, D, H). Red arrows point to cells.

A. Fresh patch fibre diameter (µm)



B. Degraded patch fibre diameter (µm) at 56 days



C.

	Fresh patch	Degraded patch
Quantiles		
100% maximum	3.542	4.531
99.5%	3.542	4.531
97.5%	2.74563	3.16235
90%	2.457	2.3574
75% quartile	2.2515	2.11075
50% median	1.8515	1.8715
25% quartile	1.6105	1.70725
10%	1.119	1.563
2.5%	0.905	1.4639
0.5%	0.549	0.987
0% minimum	0.549	0.987

Moments		
Mean (µm)	1.87325	1.9513167
Standard deviation	0.5093538	0.428636
Standard error mean	0.0464974	0.0391289
Upper 95% mean	1.9653195	2.0288959
Lower 95% mean	1.7811805	1.8739375
N	120	120

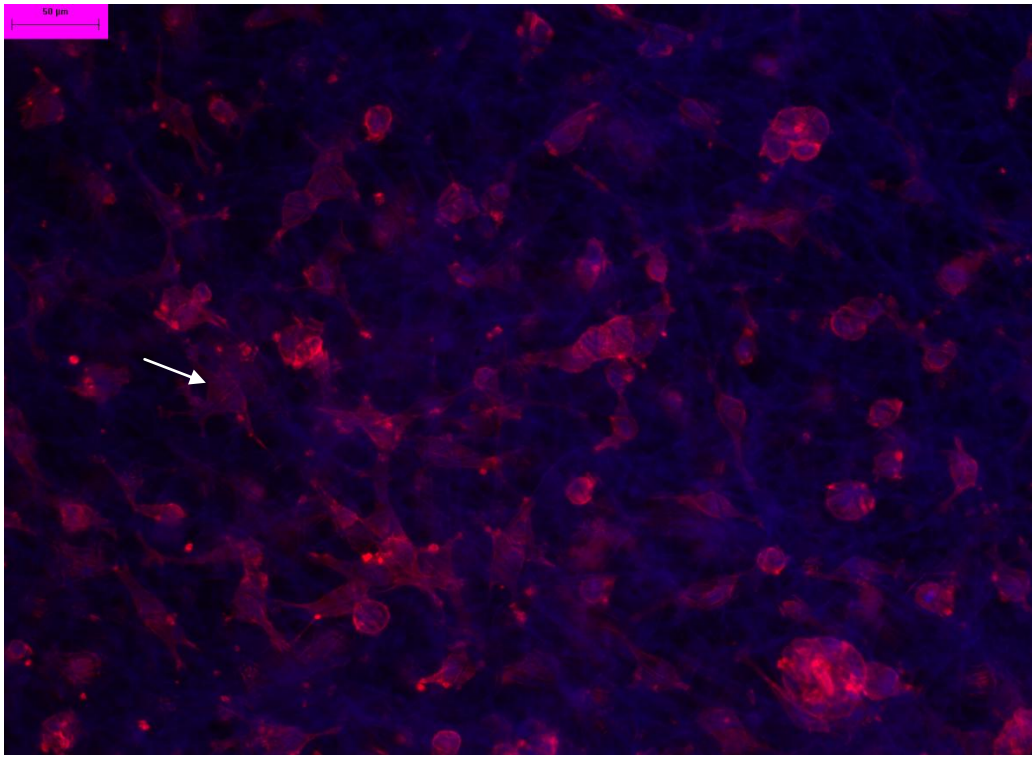
Figure 12: Graphs and table to show the comparison of diameters of fibres of PDO measured in micrometres (µm) using ImageJ (National Institutes of Health, USA). Graph A shows data from the fresh patch while Graph B shows data from a patch degraded in PBS for 56 days. Figure 11C reveals that the diameters between the 2 time points are remarkably similar with the degraded fibres mean diameter, in fact, being slightly larger.

2.3.2 Fluorescent Microscopy

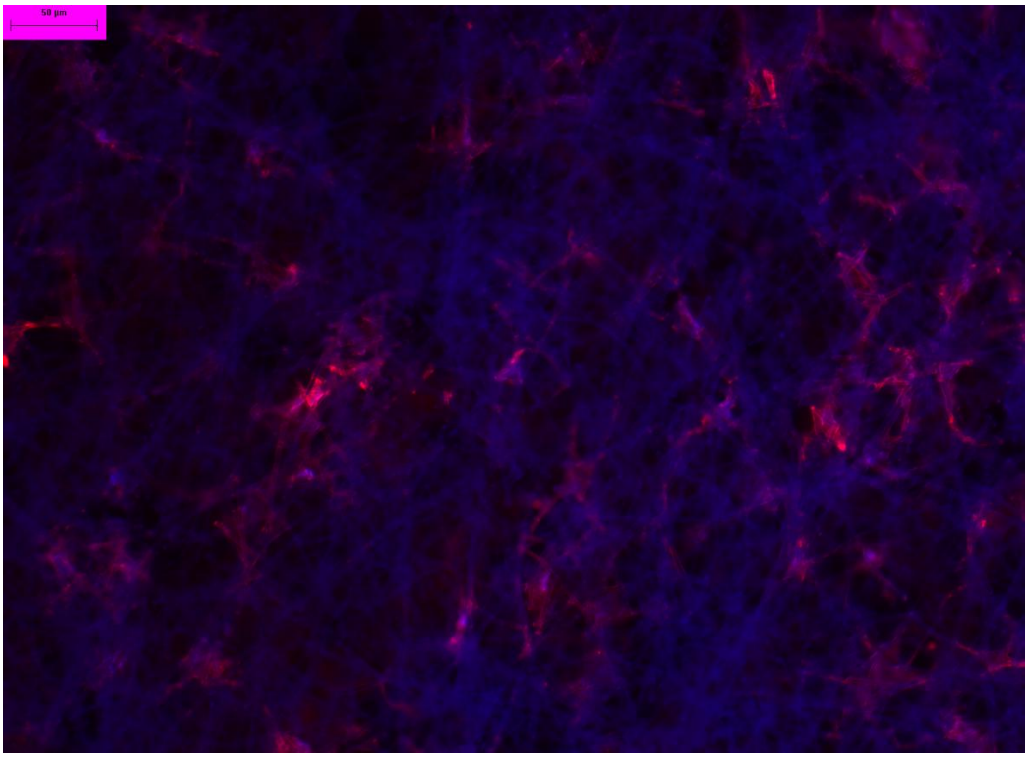
Figure 13 and Figure 14 are images of tenoblasts growing on the PDO patch, viewed after 4 weeks in culture using fluorescence microscopy. Cells were stained with DAPI and actin-phylloidin. The images clearly demonstrate cells bound to the PDO fibres. As with the ESEM images, the cells appear on the fibres in a 'star' shape where the cell body is at the centre of a number of pedicles which stretch along the fibres (see white arrow in Figure 13A). Cells that are flattened and elongated in this manner suggest strong adhesion to the PDO fibres (35).

Figure 15A and B were produced using bright light. They show the cross-sections of the broken ends of fibres as brighter dots. Unusually, the DAPI-stained cells can in fact be seen as larger bright spots (when viewed under ultra-violet light, the bright spots

corresponded to the positions of cells). The images also correspond to the ESEM images in Figure 11 (they were from the same patch), and confirm that the cells remain bound to the fibres after they began to degrade. Figure 15B shows cells attached to a segment of patch that has broken off from the main scaffold.



A



B

Figure 13: Tenoblasts incorporated into the PDO patch viewed after 4 weeks in culture. The white arrow points to a cell body.

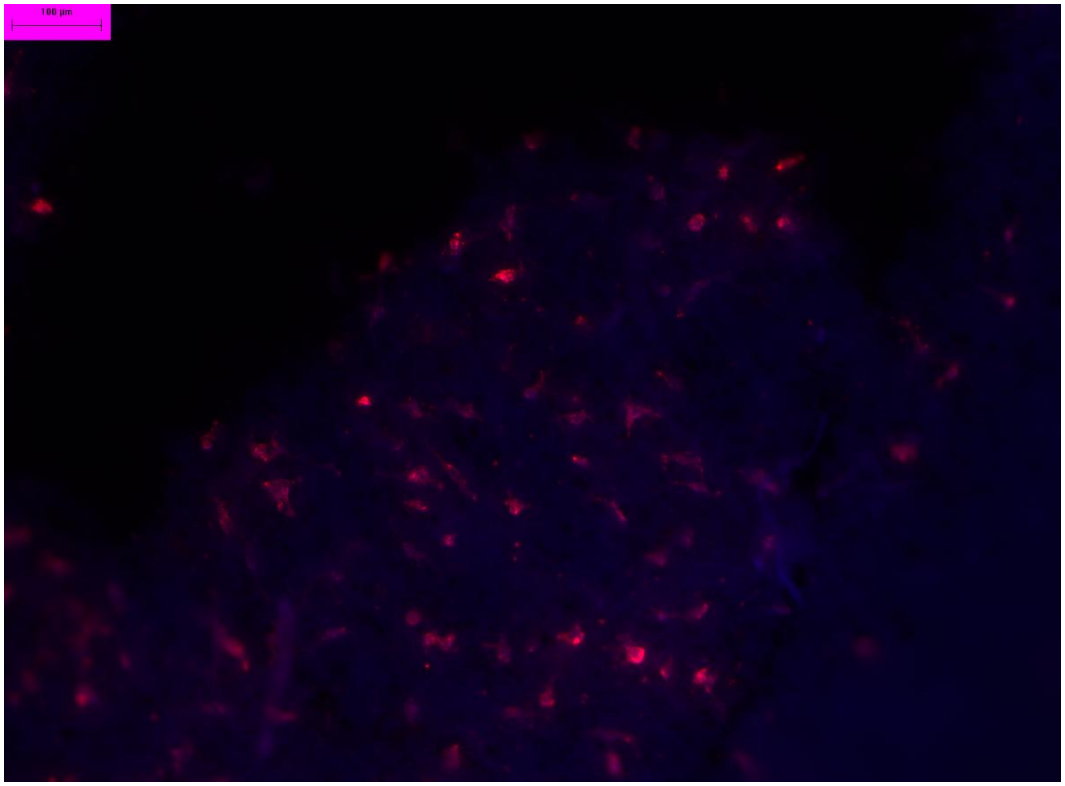
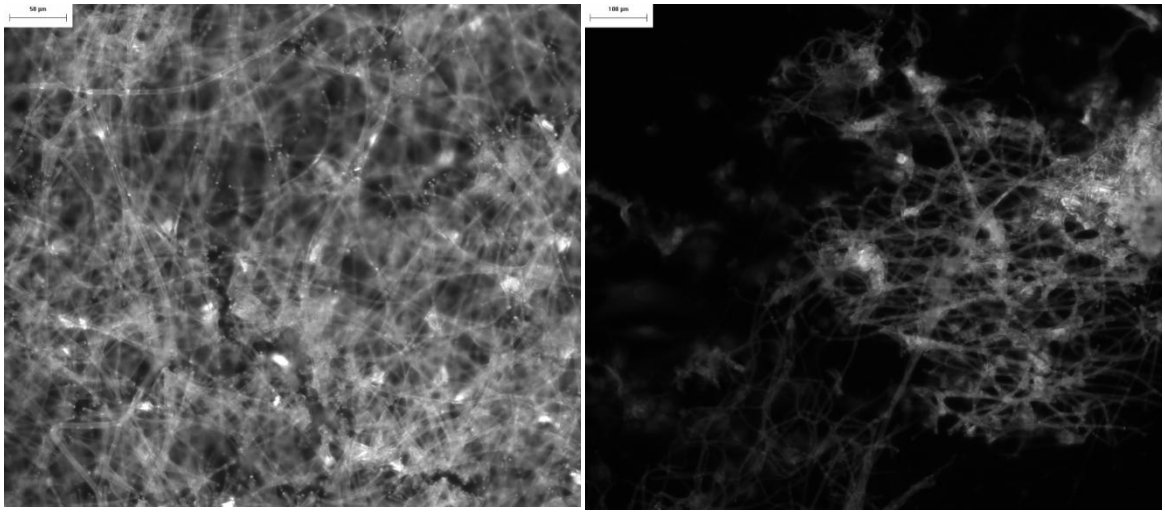


Figure 14: Cells stained red and visible on the degraded PDO patch at 4 weeks (10x).



A B

Figure 15: Tenoblasts on a PDO patch degraded for 4 weeks and stained with DAPI (20x). The cells can be seen as brighter areas, and the broken ends of fibres are visible. This corresponds to the degradation pattern seen in the ESEM images of degraded fibres. Figure 15: After 1 week x20 DAPI stain: showing cells attached to a fragment that has broken off from the main body of the patch.

2.4 Discussion

ESEM images presented in this chapter demonstrate the morphological nature of the patch as well as the breakdown process of the electrospun PDO fibres. The images of the undegraded patch show long, unbroken, randomly arranged fibres. The degraded patch images show much shorter, chopped segments, the diameter of which match those of the undegraded fibres (Figure 12). This demonstrates that the degradation starts with the shortening/breakdown of the length of the nanofibres, rather than the narrowing of their diameter. This is confirmed by Figure 12 which demonstrates the lack of difference in diameter between those fibres that were viewed fresh, and those that were viewed after 56 days degradation in PBS. It was in fact the degraded samples that had a very slightly higher mean diameter. This supports the finding that the PDO

fibres degrade by splitting along their length rather than losing material from their circumference during the first 56 days of degradation.

Perhaps the most interesting images to come from the ESEM experiment are those demonstrating the adherence of cells to the electrospun fibres. The images clearly show large numbers of cells attached to the fibres; their cytoskeleton spread along the lengths of many fibres, suggesting a firm attachment. Images of the patch after 42 days of culture reflect the biocompatibility of the patch for the tenoblasts. The spreading of cells onto the patch was also observed to be uniform: the density of cells seen on the ESEM and fluorescent microscopy images was echoed throughout the patch. There was no evidence of cells localising to a certain area of the patch.

Fluorescence images demonstrated cells on the patch for up to 4 weeks, the ESEM images further showed cells on the degradation products of the patch. Taken together, this suggests good compatibility of the patch throughout its life as a cell substrate and a robust interaction between host fibres and cells.

Using the images to evaluate morphological changes, degradation appeared to begin just prior to the 30 day point (Figure 8A demonstrates a small degree of surface erosion). By 56 days, the patch maintained some degree of macro structure, though it shed large amounts of fragments, and all long fibres had been degraded into smaller segments.

The implications of this for the use of an electrospun PDO patch *in vivo* are that the tenoblasts will thrive in the environment provided by the patch. Even as the patch degrades and sheds fragments, a proportion of the cells are expected to stay attached

to the scaffold. The hypothesised next step is that recruitment factors from the injured tendon will encourage replication and migration of repairing cells to the injury site.

Moreover it is likely that these large fragments remain localised to the area of tendon damage due to the tightly packed environment over the tendon surface. As a result, the PDO patch can still be fulfilling its role as it degrades.

2.4.1 Further work

It would be of interest to visualise matrix deposition by the tenoblasts on the patch as they grew. Matrix deposition is likely to be another important factor influencing the degradation of the patch. It is also a useful marker of how beneficial a therapy using these cells would be (36).

3 Monitoring the degradation of PDO patches using weight loss, pH and high performance liquid chromatography

3.1 Introduction

It was of interest to characterise the patch in terms of identifying how the polymeric fibres of polydioxanone degraded, and what they degraded to. Three methodologies were used in this chapter: high performance liquid chromatography (HPLC) (Chapter 3.2.3), weight loss calculation (Chapter 3.2.1), and pH measurement (Chapter 3.2.2).

Isolation and identification of the final degradation product was attempted using HPLC. This required a number of optimisation experiments (Chapters 3.2.3. to 3.2.7). Calculations of weight loss and change in the pH of the polymeric solution were also performed in order to establish the time scales in which the polydioxanone scaffold degrades.

3.1.1 PDO degradation mechanism

As seen from the ESEM images, during incubation in media, larger segments of scaffold broke off from the main structure. It was of interest to investigate this further. Sabino et al described two-stage hydrolytic degradation kinetics in polydioxanone. The paper did not specify whether their model was solely for polydioxanone, or extended to other beta-hydroxy polymers. As discussed earlier, polydioxanone is known to be a semi-crystalline polymer (15). That is, it forms mixtures of crystalline and amorphous areas and melts over a range of temperatures instead of just one melting point. The

amorphous region holds a more glass-like structure: hard, relatively brittle, and lacking any long range transitional symmetry or order, while the crystalline material shows a higher degree of order and is formed by the stacking and folding of polymer chains.

Sabino *et al* found the hydrolytic attack of the sparser amorphous areas to be a lot faster than that on the crystalline areas, and have proposed an approximate model of the detailed hydrolytic degradation of PDO (15). Sabino's model, depicted in Figure 16: , demonstrates how the two different modes of degradation, (I) and (II), meet an identical end-point at (e), when the final degradation product (proposed as glyoxylic acid) is produced.

- Mechanism (I): Faster hydrolysis of the amorphous regions.
- Mechanism (II): Slower hydrolysis of the crystalline lamellae (diffusion hindered by tight crystal formation).
- Stage (a): Fragmentation of sets of lamellae.
- Stage (b): Crystalline region hydrolysis begins at the chain folds in the lamellae's basal plane.
- Stage (c): Subsequent lamellae cleavage.
- Stage (d): Smaller crystal fragments produced.
- Stage (e): Single chains emerge from the crystals and dissolve in the PBS into a final degradation product purported to be glyoxylic acid.

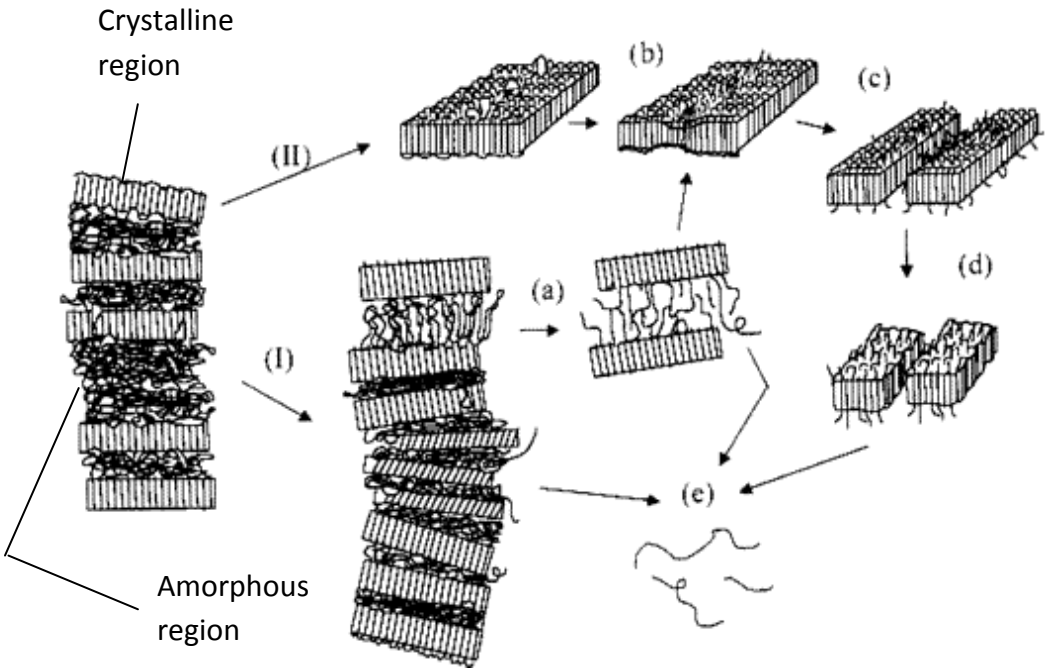


Figure 16: Proposed approximate model of the detailed degradation of PDO (This figure is courtesy of Sabino *et al* and contains modifications) (15).

Although the polymer degrades via both mechanism (I) and (II), mechanism (I) progresses more rapidly during the first weeks. One of the reasons for this is what has been termed 'cleavage-induced degradation'. This was described by Sabino *et al* (15), Zong *et al* (37), and Fu *et al* (38). It involves a rapid increase in the absolute amount of crystallinity as degradation progresses over the first 7 weeks. The rate of increase then slows down. Sabino *et al* hypothesised that the reason for this is that the initial hydrolysis of the amorphous regions removes many of the knotted and tangled chains separating the crystalline regions, thus removing conformational hindrances (15) with subsequent *de novo* crystallisation region formation. It was also noted that the increase in crystallinity slowed over time.

It was thus of interest to validate their claim that PDO degrades in two stages, by quantifying the release of the final degradation product versus the release of larger "polymer chunks". In doing so, it will be possible to ascertain not only whether there are two stages of degradation, represented by a change in speed of degradation, but also the relative constituent parts of this degradation material. This will also have implications for the toxicity of the material.

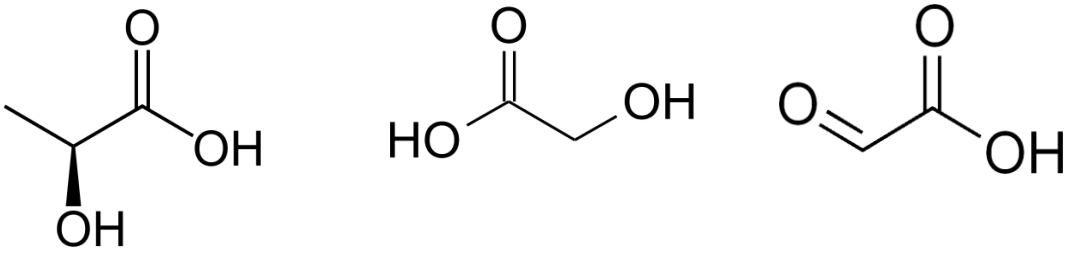
3.1.2 Polydioxanone's final degradation product

For a material to be safely implanted into a living tissue, as much information as possible should be garnered from the material in order to ascertain what effects, be they positive or negative, the material may have on the tissue and host. In the case of a biodegradeable implant, the final degradation product must be identified. As polydioxanone degrades, degradation products are released into the surrounding environment. Lanzer *et al* have stated that the monomer glyoxylic acid is the final degradation product of polydioxanone(39). Many other sources have agreed with the claim, though none have been found which experimentally demonstrate without question that glyoxylic acid is polydioxanone's final degradation product. Identifying the breakdown products is of importance because of possible tissue response to circulating exogenous particulates. An example within the orthopaedic field is cobalt-chrome ions displaced from metal-on-metal hip arthroplasties potentially causing CD8+ T-cell lymphopenia (40). It is also useful to know the identity and circulating concentrations of breakdown products so that accumulation in tissue and organs can be evaluated. This study aims to validate the claim that glyoxylic acid is polydioxanone's final degradation product.

Lactic acid, glycolic acid and glyoxylic acid are all within the family of alpha-hydroxy and carboxylic acids (41). These three compounds were therefore used to compare to the monomer of PDO in an attempt to identify the exact final degradation product. Their structures can be seen in Figure 17:

The actual molar masses of these monomers are as follows:

- Lactic acid: 90.08 g/mol
- Glycolic acid: 76.05 g/mol
- Glyoxylic acid: 74.04 g/mol



Lactic acid Glycolic acid Glyoxylic acid

Figure 17: The chemical structure of lactic acid, glycolic acid and glyoxylic acid.

3.1.3 High Performance Liquid Chromatography (HPLC)

Chromatography is the process of separating mixtures of compounds. A mixture dissolved in a 'mobile phase' is passed through a 'stationary phase'. This separates the analyte from other molecules in the mixture, allowing analysis of its constituents.

The most powerful chromatographic technique involves the sample passing through a column containing appropriate particles (the stationary phase). These particles are the

chromatographic packing material. A solvent (the mobile phase) flows through the column carrying the sample with it. The different compounds in the sample are then separated by travelling at different speeds through the device.

High performance liquid chromatography (HPLC) is an extension of these basic principles. Smaller particle sizes are required to provide a higher separation power and greater ability to differentiate between compounds. However, smaller particles in the chromatographic packing material require higher pressures to create the desired solvent flow rate due to their greater resistance to flow. Consequently, HPLC was born out of the need to separate, identify and quantify any compounds present and any sample that can be dissolved in a solvent. HPLC can easily identify compounds in concentrations of parts per trillion.

In HPLC, the solvent, or mobile phase (because it moves through the column), is held in a reservoir. A high pressure pump (or solvent manager) delivers the mobile phase at a controlled variable rate measured in millilitres per minute. An injector (or sample manager) introduces the sample into the mobile phase stream, and the solution then passes into the chromatographic packing material (stationary phase) contained within the column. As the separated column bands elute from the column, they are identified by a detector. The mobile phase exits the column and can be collected or discarded as waste. Figure 18: provides a simplified schematic graphic of the HPLC process.

The detector is connected to a computer terminal that records the electronic signal generated by the detector and generates a chromatogram on its display, enabling identification and quantification of a compound's constituents. Detectors can be based

on ultra-violet light absorption, fluorescence detection, evaporative-light-scattering detection, or a combination of the three. For this experiment, an ultra-violet light detector was used.

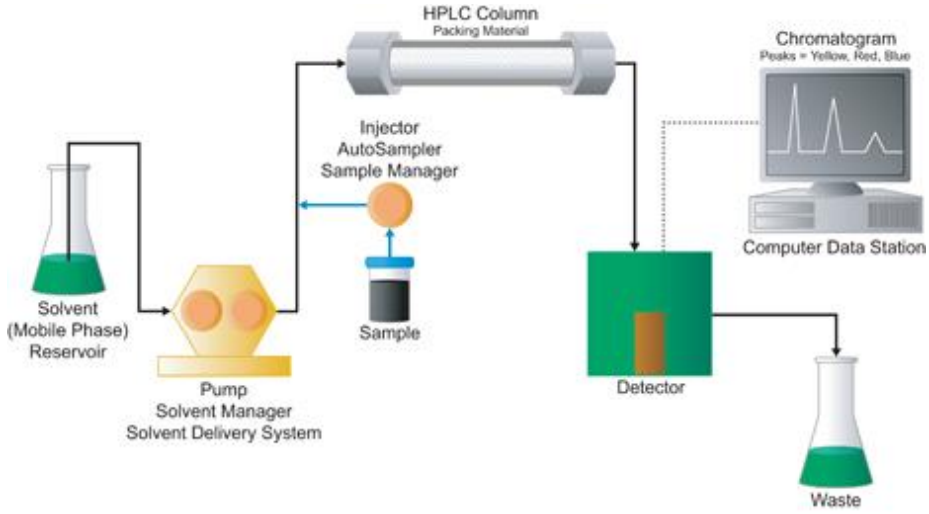


Figure 18: A schematic representation of an HPLC apparatus. Figure courtesy of https://waters.com/waters/nav.htm?cid=10049055

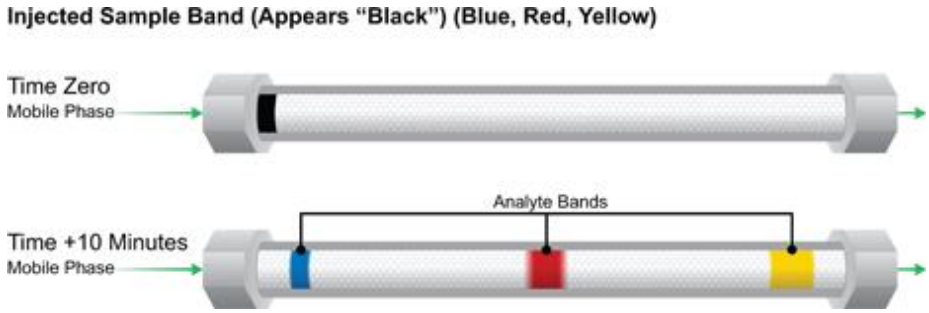


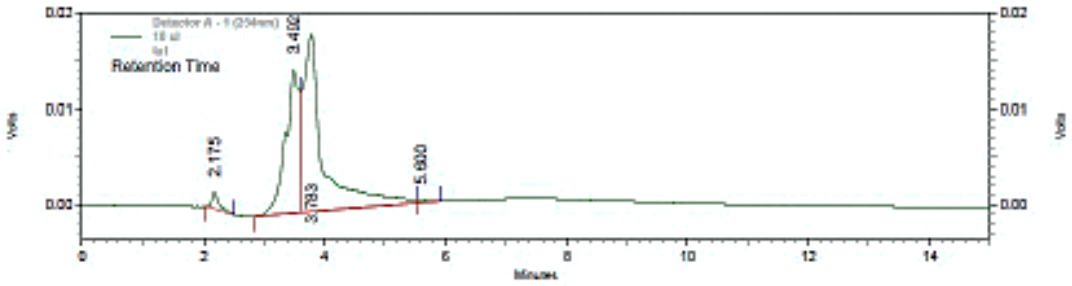
Figure 19: A schematic representation of compounds passing through an HPLC column and being separated according to their affinity to the static phase. Figure courtesy of https://waters.com/waters/nav.htm?cid=10049055.

Figure 19 demonstrates how the chromatographic process works. The colours are helpful to visualise the process, though in reality, the compounds are colourless and the walls of the column opaque so a detector is needed to see the compounds as they elute. At time zero (Figure 18:), the mixture of blue, red and yellow compounds appears black as it enters the column. As the mobile phase flows past the packing material particles, individual compounds are attracted in varying strengths to the stationary phase and consequently move in different bands at different speeds. There is competition between the mobile and stationary phases for the compounds' affections. For instance, the yellow compound is attracted to the mobile phase the most and consequently moves at a faster rate through the column, closest to the speed of the mobile phase itself. In contrast, the blue compound prefers the stationary phase and has a resultant slower speed through the column as it is more adherent to the packing material. It is said to be the most retained compound.

Since each compound moves through the stationary phase at a different speed due to their unique molecular weight and charge, they can be separated chromatographically.

The chromatogram produced once the detector has identified the present compounds is a representation of the chromatographical separation in the column (Figure 20:). The chromatogram shows detector response signal (y-axis) over time (x-axis). Each peak on the chromatogram represents the detector response for a different compound. The baseline of the chromatogram represents pure mobile phase passing through the flow cell over time. A thicker peak on a chromatogram indicates that a

compound took longer to elute and was hence retained longer in the column due to an affinity for the stationary phase (42).



Detector A - 1 (254nm)

Pk #	Retention Time	Area	Area %	Height	Height %
1	2.175	14069	2.071	1754	4.968
2	3.492	228368	33.615	14845	42.044
3	3.783	433194	63.765	18411	52.144
4	5.600	3726	0.548	298	0.844

Figure 20: An example of a chromatogram produced by high performance liquid chromatography.

Thus, compounds can be identified by using reference standards. Identical retention times (the time point of a peak formed on the chromatogram) indicate identical compounds. In a similar way, concentrations of compounds in different samples can be compared by quantifying the area under the compounds peak. The more concentrated the compound is, the stronger the signal, and the greater the peak height above the baseline. The area under the peak is automatically calculated by the computer. In this study, the area under the curve has been used as an indication of concentration (42).

3.1.4 Weight Loss and pH

Whilst qualitative information on the degradation of PDO was gained from microscopic observation of the morphology of samples in Chapter 1, quantitative data was

obtained using weight loss as a marker of degradation, which was measured until the patch disintegrated and could not be handled.

Although the remit of this thesis is wholly in-vitro, the implications of degradation products for in-vivo applications of the PDO patch are important. Since cells are to be incorporated into the electrospun fibres, a drop in pH due to accumulation of acidic degradation products may cause necrosis (43). However, the in-vivo environment in the body is continuously in flux, and accumulation may only be short term. Thus, it was hypothesised that the accumulation of acid under static conditions may provide a 'worst-case scenario', while accumulation under dynamic conditions (replacing the buffer at regular intervals) may reflect better the in-vivo environment.

The effect that dynamic conditions have on the concentration of degradation products and the speed of degradation was thus investigated in this chapter. It is hypothesised that under dynamic conditions, where the buffer solution is being frequently renewed or 'flushed' away, the buffering power will be increased and the subsequent lower acidity or higher pH of the medium will result in slower hydrolysis of the polymer molecules.

Sabino et al have performed similar experiments on poly(*p*-dioxanone) but did not replace the buffer solution. They hypothesised that if a regeneration of the buffer system had been performed (as in the dynamic arm of our experiment), the degradation rate may have been slower. This is due to the self-perpetuating nature of hydrolysis - the 'snow-ball effect' - in an acidic environment, where acidic end-groups increase the hydrophilicity and catalyse further degradation (16). When using no

buffering solution (for instance if using distilled water as a hydrolysis medium), the rising acidity of the medium normally accelerates the polymer hydrolysis (15).

The aim of the pH experiment was to employ similar distinctions as the HPLC experiment with regards to a static and a dynamic experiment arm (as described in 3.1.4). The static arm measures the pH of the solution containing the degrading patch without replacing the medium. The dynamic arm involves replacing the PBS after measuring the pH. This method aims to highlight differences between an *in vitro* environment, and a more realistic *in vivo* environment where the physiological fluid in which the implant is to be bathed is replaced constantly. Though the rotator cuff tendons are not highly vascularised, even small amounts of blood flow and movements of the joint cause fluid to track into, out of and around the joint. A dynamic set up *in vitro* should give a better reflection of the pH around the PDO patch *in vivo*.

3.1.5 Aim

The first aim of the study presented in this chapter is to investigate whether glyoxylic acid is the final degradation product of polydioxanone *in vitro* (Chapter 3.2.3). If it is, it cannot be assumed that it is the sole breakdown product. HPLC experimentation is the method used to investigate the final degradation product of polydioxanone.

The second objective is to quantify the concentrations of the degradation products over time as the scaffold degrades (Chapters 3.2.1-2 and 6) This may help assess the safety of the patch, as well as understand the degradation mechanism. Change in pH of the polymeric solution, and weight loss of the scaffold patch, are used as surrogate

markers of degradation which contribute to our understanding of polydioxanone's degradation.

3.2 Materials and Methods

3.2.1 Weight loss

Electrospun polydioxanone (Produced by Nanoforce) was tested along with controls of PDSII suture (Ethicon) and silk (Oxford Biomaterials). Three samples of each material were used, and the mean was calculated for each material. The samples were sterilised in 70% ethanol to prevent microbial growth which may alter the pH. To record the rate of weight loss, test tubes were weighed using a Mettler AE 200 electronic analytical balance with 0.1mg readability before having sterile samples added to them. Sterile phosphate buffered saline (PBS, Biowhittaker/Lonza) was then added in a ratio of 1ml per 10mg of sample. The samples were incubated at 37^{o}C and 5% CO_2. They were removed at day 35, 56 and 91 before being dried in an oven at 58^{o}C for 24 hours. They were then re-weighed before being re-sterilised for further incubation. The percentage weight loss of polydioxanone samples was calculated.

The same experiment was repeated with PDO patch samples that were incubated for longer periods without being weighed. These samples were left to incubate for over 5 weeks before being re-weighed.

3.2.2 pH

Two polydioxanone patches were weighed and placed in test tubes containing phosphate buffered solution at a concentration of 20mg/ml. The initial pH was measured using a pH meter (Hanna Instruments HI2210 pH meter). Three readings

were taken for each and the mean was calculated. The test tubes were incubated at 37^{o}C and removed at intervals to re-measure the pH.

3.2.3 HPLC study to identify polydioxanone's final degradation product

An experiment was set up where the three compounds detailed in 3.1.6. (lactic acid, glycolic acid and glyoxylic acid) and the degradation product of polydioxanone were analysed using HPLC. PDO was degraded using hydrochloric acid. Each compound was analysed individually (as described in more detail in section 3.2.5), then in paired mixtures, then finally in one solution all together. The aim was to achieve identifiable peaks for each compound in a mixture. The peaks could be compared to see if the breakdown products of polydioxanone correspond to glyoxylic acid, lactic acid, or glycolic acid. Three samples of each compound were analysed, and the mean calculated for each.

3.2.4 Static and dynamic experiments

For all experiments carried out in this chapter, there were two arms: a Dynamic and a Static arm (described fully in Chapter 3.1.4). The Dynamic arm is intended to represent the *in vivo* environment where a degree of blood flow through the area means that the liquid environment directly over the patch will be constantly replaced. The Static arm represents the conditions present when all the degradation products accumulate in solution. For each experiment, 3 samples were analysed, and the mean calculated for each.

3.2.5 HPLC analysis: optimisation experiment

In order to use HPLC to identify and quantify the degradation products of PDO, it was required to optimise the method for running samples through the apparatus and obtaining repeatable, valid results. The column used for this application requires a mobile pH phase of between 2 and 7.5, because of the silica static phase which may become damaged at extreme pH. Experiments involving the buffering of all solutions were performed to maintain the samples within this ideal pH range. However, as buffering the samples yielded poor results and was inconsistent between samples, it was decided to run samples unbuffered. On occasion, the pH of the solution will have strayed outside of the desired range, but after discussion with the manufacturer, it was expected that due to small sample volumes this had not damaged the column.

To comparatively quantify larger fragments of the patch versus smaller degradation product, samples were filtered using a 0.45µm filter to separate the larger degradation products. Here, large fragments retained above the 0.45µm filter were named “retentate” while the smaller degradation products collected after filtration were named “filtrate”.

For quantification, it was necessary to hydrolyse both retentate and filtrate samples to their final degradation products. Concentrated sodium hydroxide (NaOH) is a strong hydrolysing agent and was used in this instance. Hydrolysis is a process by which a water molecule is added to a compound resulting in the split of that compound into two parts as well as the splitting of the water molecule. A strong acid or base is usually

needed to catalyse the reaction, in this case NaOH. Thus, after filtration, 5M NaOH was added to all samples to a concentration of 0.45M.

After filtration, to collect the retentate, 100µl of PBS was added to the filter insert, and 10µl of NaOH was then added to the PBS in order to dissolve the remaining fragments before detection by HPLC.

A protocol optimisation was performed to determine optimal incubation time in NaOH to complete hydrolysis. To do so, samples of PDO were placed in a PBS solution in a concentration of 20mg/ml. A range of volumes of 5M NaOH were added to this solution in the following final concentrations: 1M, 0.5M and 0.25M. The samples were then mixed in a vortex, and observed for visible disintegration. This was used as a method for estimating which volume of NaOH to use. The 1M NaOH sample was completely dissolved in minutes. Samples at concentration range 0.5 to 0.25M took from 2 hours, to overnight. To minimise sample dilution and to avoid damaging the silica HPLC column 0.25M NaOH was selected for the experiment since it had visibly dissolved the sample within 3 hours, and would only dilute a 100µl sample by 10%.

To optimise the exact incubation time prior to HPLC analysis, samples were incubated in PBS in a concentration of 20mg/ml, with 10ul NaOH added. They were left on a stirring device for 2, 6, and 30 hours, before analysis using the HPLC apparatus protocol.

3.2.6 HPLC analysis: degradation kinetics experiment

For the main degradation study, two polydioxanone patches were sterilised in 70% ethanol and then incubated in phosphate buffered solution (PBS) at 37^0C at a

concentration of 20mg/ml. This concentration was used because if 20-30% of the patch degraded at this concentration, according to previous optimisation experiments this would breach the detection threshold of the HPLC apparatus. At specific time points, 20µl aliquots of the solution were removed for HPLC analysis. One patch was incubated under dynamic conditions and the other under static conditions, as explained in section 3.2.4. As controls, PDSII, Ethibond and Ethisorb were used. Ethibond is a non-degradeable suture while the PDO and Ethisorb sutures are degradeable. The rationale behind using these controls is to demonstrate that the changes in the chromatograms produced by HPLC are not due to contamination of the PBS solution itself, but to material degradation.

At defined time points, aliquots were removed from well-mixed sample solutions, frozen and stored at -80^{0}C. For the static experiment and the controls, 100µl of solution was removed and replaced by 100µl sterile PBS. For the dynamic experiment, all solution was removed and replaced with sterile PBS.

Since in both the Static and Control arms of the experiment 100ul aliquots were removed and replaced with fresh PBS, their concentrations were reduced slightly during the course of the experiment. This was unavoidable since the sample could not be retrieved unaltered from the HPLC process. This was taken into account when analysing the results.

At the time of the analysis, samples were defrosted in a water-bath before being pipetted into 0.45µm centrifuge filters (VectaSpin-Micro 2ml; outer tube polypropylene; 400ul inner filter insert; 0.45um pore size; Whatman). The pH of the

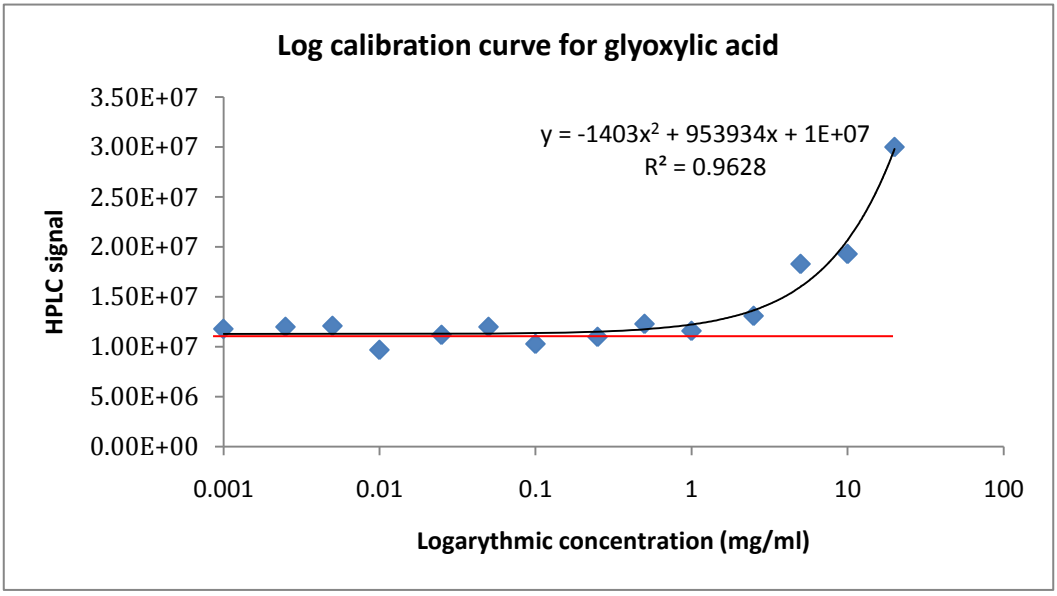
samples was measured using litmus paper and recorded in order to follow changes in pH throughout the experiment. The filters were then centrifuged at 14,000rpm for 2 minutes.

To avoid damaging the column, and following discussion with the manufacturer (HiChrom Ltd; Berkshire; England), it was established that small quantities of acid or alkali would be safe to run providing the column was flushed sufficiently with eluent before and after each run. Consequently, the pH of the filtrate was measured using litmus paper, and subsequently buffered using 16% HCl in 30ul aliquots. Once the concentration has been elicited by applying the signal from the chromatogram to the calibration curve, the volume of HCl will be theoretically removed from the concentration and the concentration recalculated.

3.2.7 HPLC analysis: calibration curve formation

To calculate concentrations and identify detection limits, a calibration curve was prepared for glyoxylic acid (Sigma-Aldrich, St Louis, USA). This produced a range of chromatographic peaks of concentrations and is shown in Figure 21. The R^2 value of 0.9607 calculated from the slope demonstrates the linear relationship between concentration and area under the curve.

A.



B.

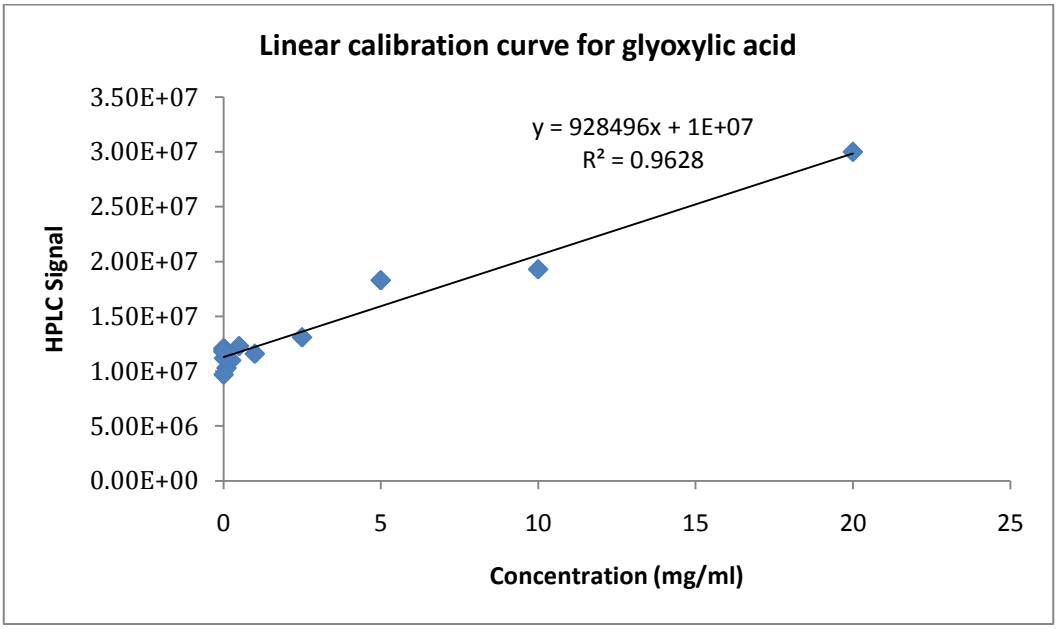


Figure 21: Calibration curves for glyoxylic acid. A: Logarithmic calibration curve showing detection threshold line. The red line represents the approximate threshold of detection by the HPLC apparatus (at a signal of 1.2×10^7). The black line bisects the points of the calibration curve and represents an R^2 value of 0.96. B: Calibration curve showing linear regression.

To prepare standards for the calibration curve, 200mg of Glyoxylic acid monohydrate was dissolved in 2ml of PBS to a final concentration of 1.07M. This was then diluted to 14 concentrations ranging from 20mg/ml to 0.001mg/ml.

Each sample was buffered with 16% hydrochloric acid (HCl) solution to a pH of between 3.5 and 6.5. pH was verified using litmus paper. Samples were buffered individually and upon addition of HCl the concentrations of the individual solutions were re-calculated. Buffered samples were then each placed in a sterile 0.22um centrifuge filter (Millipore Ultrafree Centrafugal filters; Durapore) and centrifuged for 3 minutes at 14,000 rpm. The filtrate was pipetted into HPLC sample tubes and capped.

The column used was an Inertsil ODS2 (Hichrom) with a length of 25cm and an internal diameter of 4.6mm. Before running any samples, the HPLC device was flushed with filtered MilliQ water, and acetonitrile. Before every sample, a run of 80% Acetonitrile: 20% filtered MilliQ water was performed to flush the column.

3.2.8 HPLC analysis: dynamic and static experiments

For the dynamic/static experiment 3 PDO patches were sterilised in 70% ethanol and incubated in test tubes at 37°C in sterile PBS in a ratio of 20mg material in 1ml PBS.

- Static experiment: 23.04mg PDO patch incubated in 1.152ml PBS
- Dynamic experiment: 21.26mg PDO patch in 1.063ml PBS
- Controls:
    - 23.34mg PDO suture in 1.167ml PBS
    - 176.03mg Ethibond in 8.8015ml PBS
    - 93.94mg Ethisorb in 4.697ml PBS

- Ethibond is a non-degradeable suture while the PDSII and Ethisorb sutures are degradeable. The rationale behind using these controls is to demonstrate that the changes in the chromatograms produced by HPLC are not due to degradation of the PBS solution itself, but due to the material in solution.

At defined time points, beginning with 24 hours, aliquots were removed from each sample solution after shaking the sample to mix the solution. These aliquots were frozen and stored at -800C.

- Static experiment: 100µl solution removed; 100µl sterile PBS replaced.
- Dynamic experiment: all solution removed; 1.063ml PBS replaced.
- Control: 100µl solution removed; 100µl sterile PBS replaced.

Since in both the Static and Control arms of the experiment 100µl aliquots were removed and replaced with fresh PBS, their concentration were reduced slightly during the course of the experiment. This was unavoidable since the sample could not be retrieved unaltered from the HPLC process. This must be taken into account when analysing the results.

Prior to HPLC runs, samples were defrosted in a water-bath and pipetted into 0.45µm centrifuge filters (VectaSpin-Micro 2ml; outer tube polypropylene; 400µl inner filter insert; 0.45µm pore size; Whatman). The pH of the samples was measured using litmus paper for use as data for the pH experiment described in a later section. The filters were then centrifuged at 14,000rpm for 2minutes.

Before each set of HPLC runs, the system was flushed with filtered MilliQ and acetonitrile for 2 hours. Before each sample was processed, a run through of eluent (80% acetonitrile: 20% filtered MilliQ water) was used to clean the column. This produced more accurate results due to elimination of any residue from the previous sample. The filter insert containing the retentate was then filled with 500ul of NaOH in order to fully degrade the remaining polymer. Each insert was then placed in an empty filter and centrifuged as before. The sample was then buffered and run through the HPLC protocol as described above.

3.2.9 Threshold of detection

In HPLC analysis, the compound being assessed is not retained within the column, but instead is flushed out of the column with the eluent and detected by the UV detector. Since the compound being assessed is in solution with the mobile phase, the peak that is seen on the chromatogram for the monomer is merely the cumulative signal from the mobile phase and the monomer. As a result, the signal produced from an injection peak must be identified. This peak is formed from a sample of the waste mobile phase that is collected from the waste pipe. This is run through the apparatus to obtain a signal, below which the monomer is undetectable. This provides the threshold of detection and is an unavoidable barrier to calculating very small concentrations of glyoxylic acid. From the calibration curve, the threshold of detection was calculated to be at approximately 1.2×10^{7} (See **Figure 21**). Below this level a distinction cannot be made between the acetonitrile/water eluent and the monomer.

3.3 Results

3.3.1 Weight loss

Figure 22 shows the change in % weight after a 91 day period. As can be seen, the silk sutures did not lose weight, whilst the PDSII sutures lost approximately 52% of its weight by day 91.

Significant weight loss begins to occur at approximately the 4 week mark. Interestingly, this corresponds with the findings of Figure 23. This shows how both the PDSII suture and electrospun PDO patch begin to shed significant weight at approximately the same point: the 4 week mark. The PDO patch lost weight faster than the suture with 46% of the original weight remaining after 56 days, compared to 81% of the suture's weight remaining.

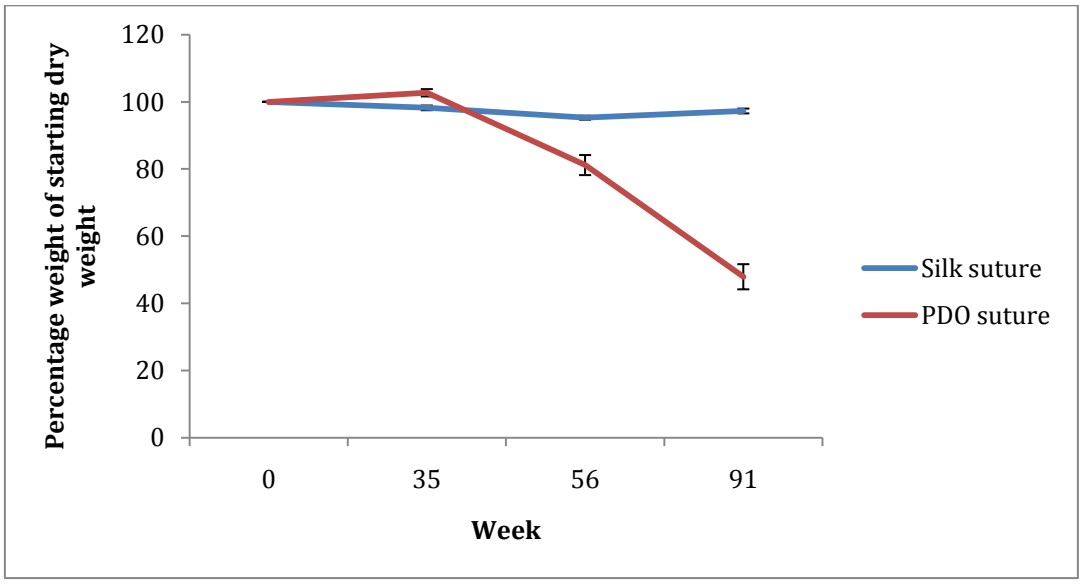


Figure 22: Weight loss of PDSII and silk sutures over 91 days. (Black error bars represent standard error from the mean).

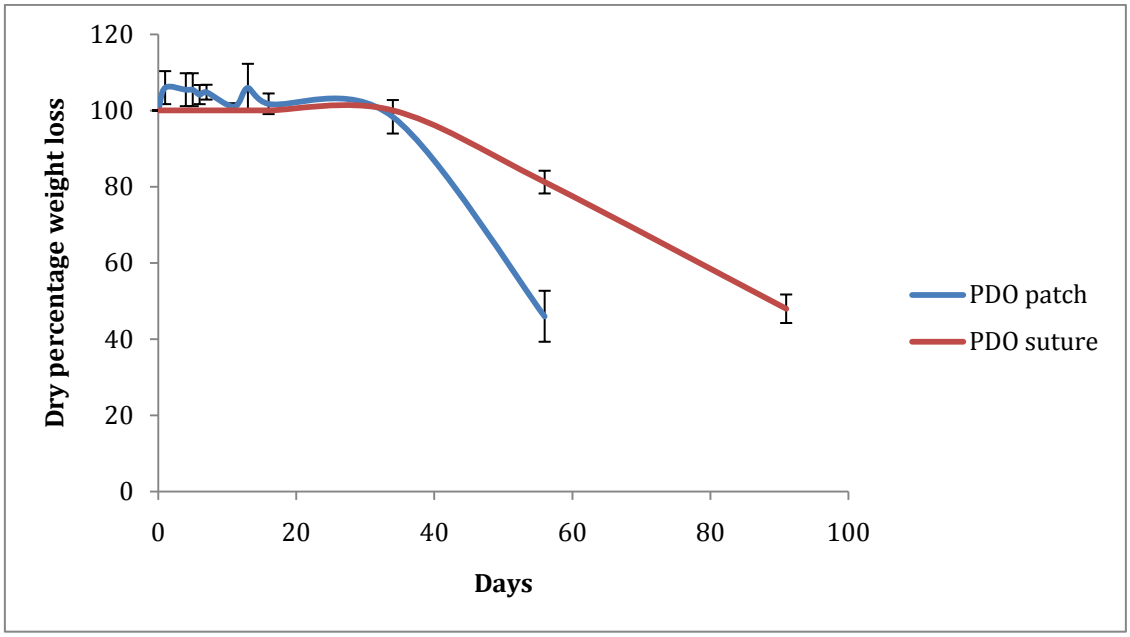


Figure 23: The percentage weight loss of PDO patch and a PDSII suture over 91 days. (Black error bars represent standard error from the mean).

3.3.2 pH

Figure 24 demonstrates the difference between the static and dynamic experiments in terms of pH. Over 47 days incubation in PBS, the dynamic experiment, in which the buffer solution was replaced at each timing point, showed a pH that remained relatively unchanged. The static experiment, in which the solvent was maintained throughout the duration of the experiment, shows a continual fall in pH as hydrolysis of the polydioxanone polymer takes place.

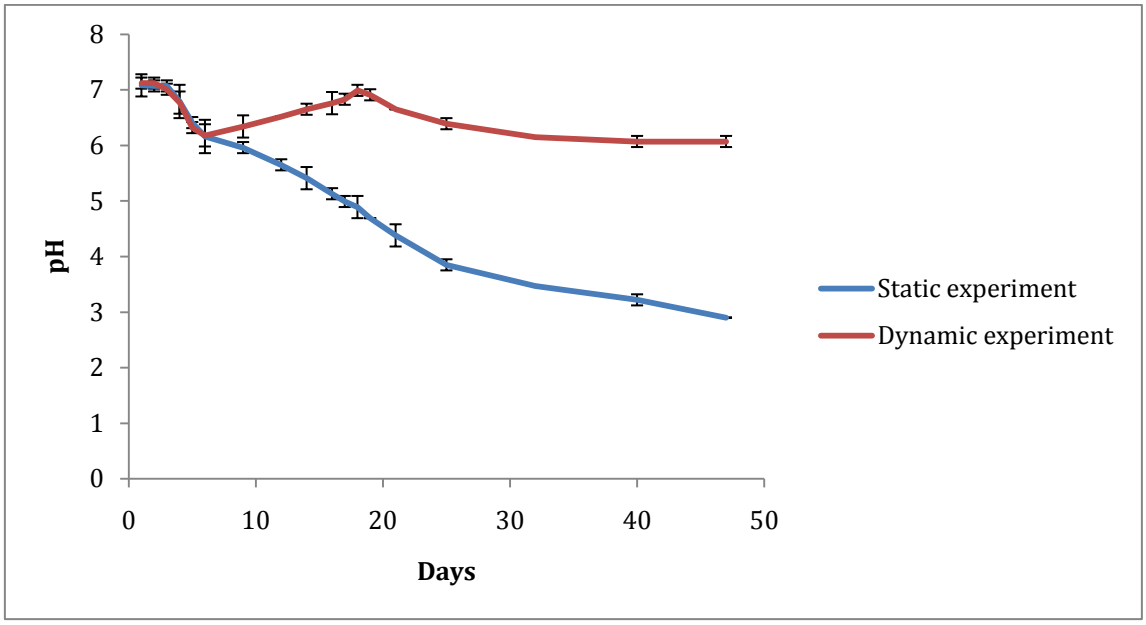
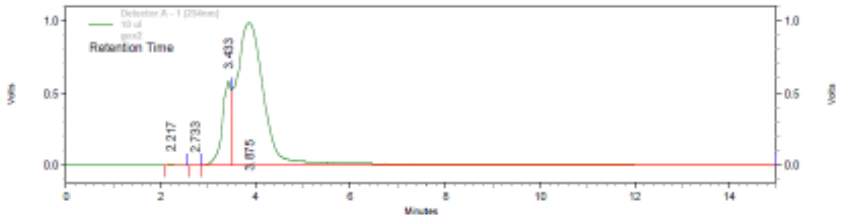


Figure 24: Change in the pH of the PBS incubation solution containing 20mg PDO patch over 47 days. (Black error bars represent standard error from the mean).

3.3.3 Results of study to define polydioxanone's final degradation product

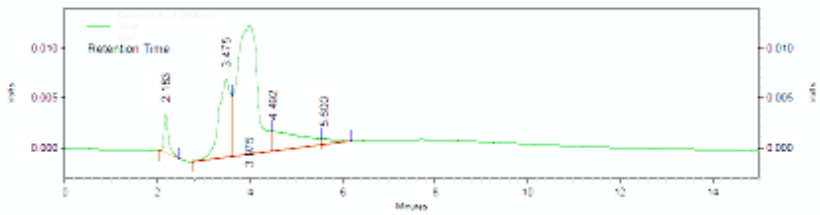
A.



Detector A - 1 (254nm)

Pk #	Retention Time	Area	Area %	Height	Height %
1	2.217	31524	0.066	5847	0.372
2	2.733	6579	0.014	884	0.056
3	3.433	7415907	15.602	579310	36.815
4	3.875	40078694	84.318	987521	62.757

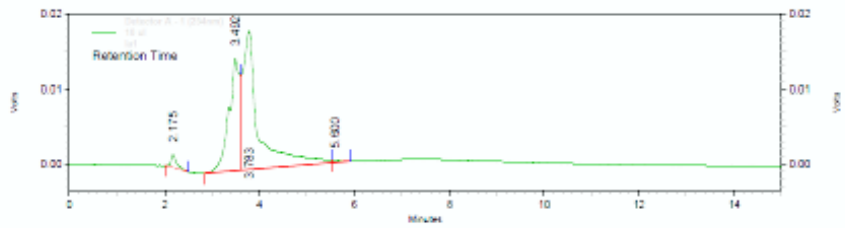
B.



Detector A - 1 (254nm)

Pk #	Retention Time	Area	Area %	Height	Height %
1	2.183	25587	3.901	5810	14.033
2	3.475	137441	20.953	7793	28.702
3	3.975	397474	60.594	12991	47.847
4	4.492	83818	12.778	1987	7.245
5	5.600	11640	1.774	590	2.173

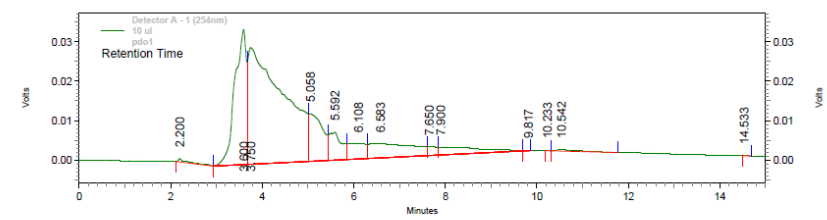
C.



Detector A - 1 (254nm)

Pk #	Retention Time	Area	Area %	Height	Height %
1	2.175	14069	2.071	1754	4.968
2	3.492	228368	33.615	14845	42.044
3	3.783	433194	63.765	18411	52.144
4	5.600	3726	0.548	298	0.844

D.



Detector A - 1 (254nm)

Pk #	Retention Time	Area	Area %	Height	Height %
1	2.200	10948	0.357	815	0.853
2	3.600	591654	19.295	34230	35.808
3	3.750	1586490	51.740	29548	30.911
4	5.058	238290	7.771	12010	12.564
5	5.592	140177	4.572	7042	7.367
6	6.108	102149	3.331	3788	3.963
7	6.583	235808	7.690	3533	3.696
8	7.650	31628	1.031	2176	2.276
9	7.900	115911	3.780	1995	2.087
10	9.817	747	0.024	49	0.051
11	10.233	223	0.007	45	0.047
12	10.542	12147	0.396	337	0.353
13	14.533	129	0.004	24	0.025

Figure 25: HPLC chromatograms for glyoxylic acid (A), glycolic acid (B), lactic acid (C), and the polydioxanone degradation product (C). Note each peak is given a corresponding time in minutes e.g. 5.058. In the table below each graph, each peak time corresponds to an area under the curve, which correlates with the concentration of the detected compound. The 4 graphs demonstrate that all 4 compounds generated 2 peaks at very similar time points: approximately 3.5 and 3.9 minutes.

The graph in **Figure 26** demonstrates the mean time point at which each of the four compounds were detected by the HPLC apparatus.

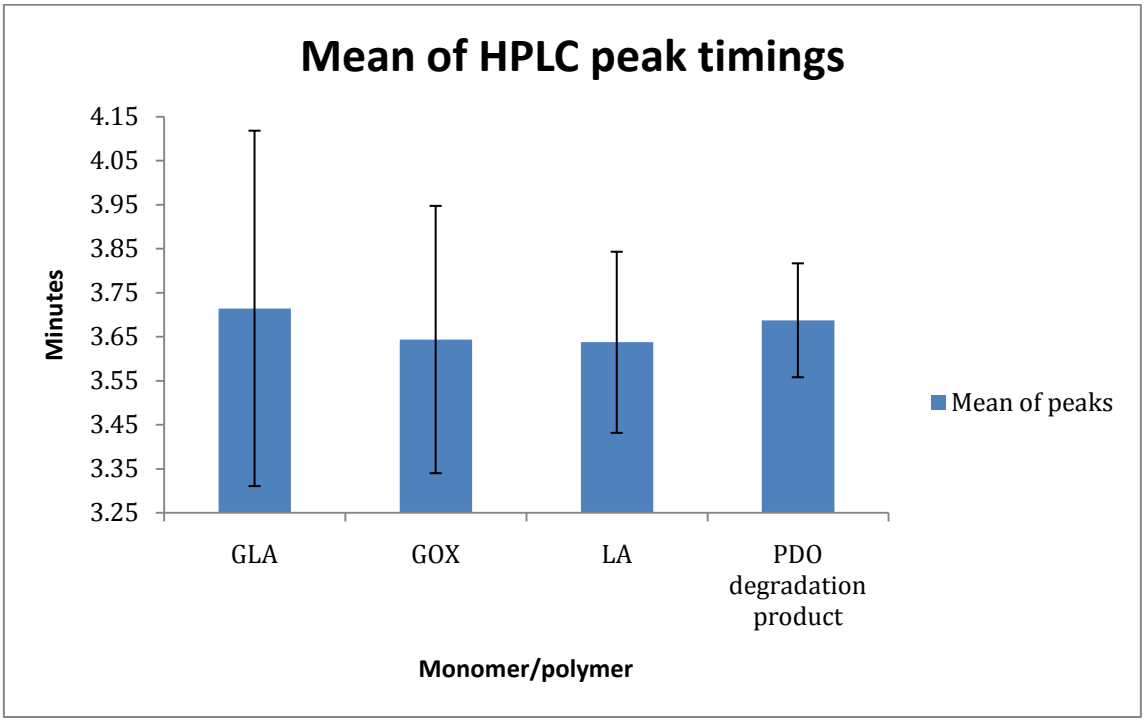


Figure 26: The mean chromatographic peaks of three monomers (GLA: glycolic acid, GOX: glyoxylic acid, LA: lactic acid) and the degradation product of PDO (all concentrations were 20mg/ml). (Black error bars represent standard error from the mean).

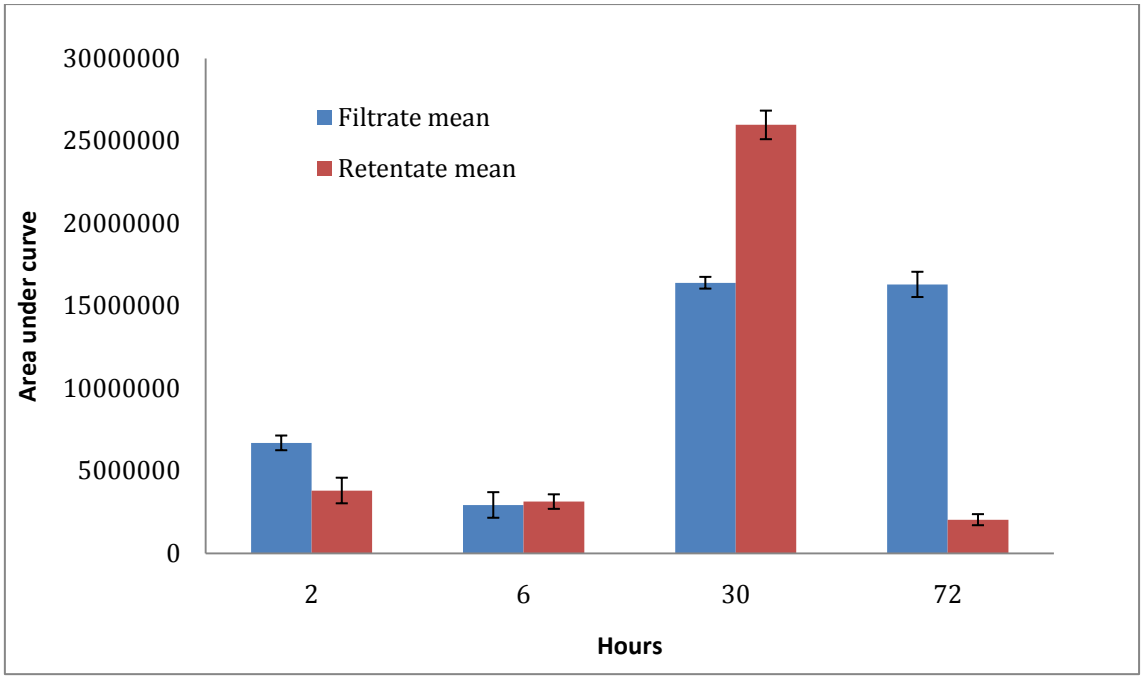


Figure 27: The chromatographic signal generation of polydioxanone solutions after different lengths of hydrolysis in NaOH. (Black error bars represent standard deviation from the mean).

3.3.4 Results of HPLC optimisation study and degradation kinetics study

Figure 27 demonstrates the changes in signal generated by the samples incubated in NaOH for different durations. The retentate getting lower after 72 days is a seemingly anomalous result, without which the graph demonstrates that there is no significant increase in signal between sample left for 30 hours and for 3 days. The reasons behind the anomalous result are intriguing. The breakdown products may be aggregating to larger particles that are not subsequently filtered. Even smaller, undetectable breakdown products may be being formed. Further investigation is required to decipher the cause of this.

Figure 28 and Figure 29 show the cumulative signal that is generated from the samples when passed through the HPLC apparatus at various time points. Figure 28 shows the

signal for the filtrate of each sample. Figure 29 shows the signal for the retentate of each sample after the initial filtration.

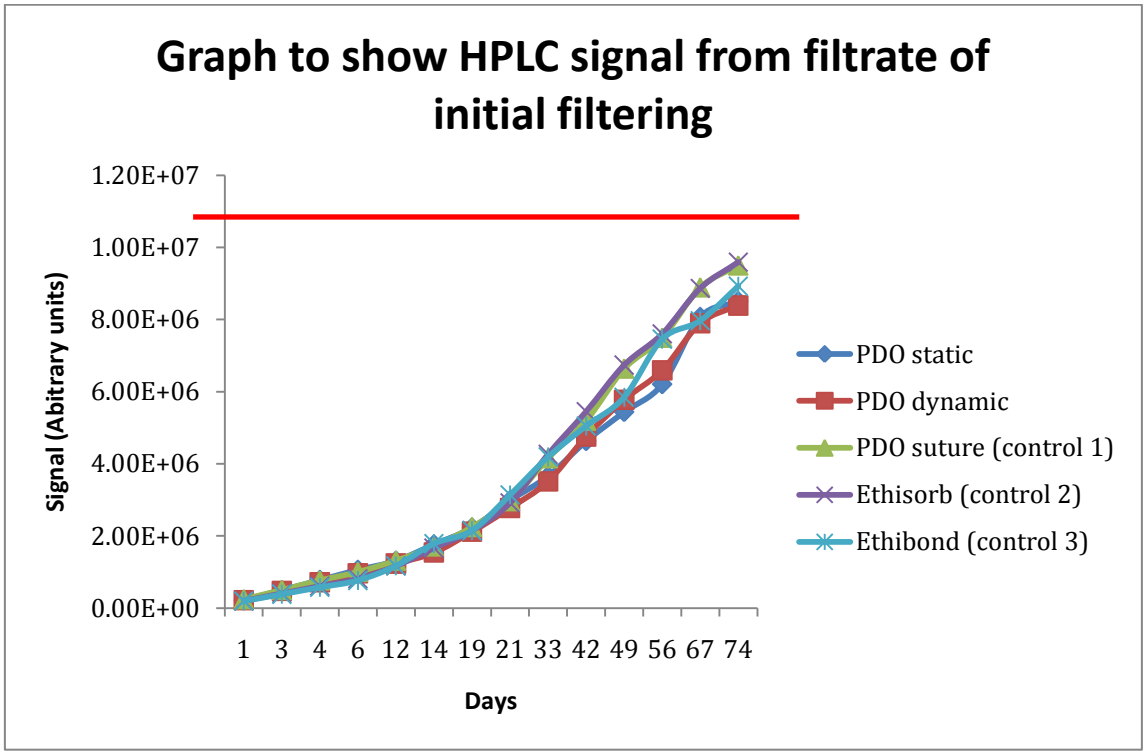


Figure 28: Cumulative HPLC signal generated from the filtrate (in terms of areas under the peak). The straight red line represents the threshold of detection. This demonstrates that none of the filtrates reach the threshold of detection.

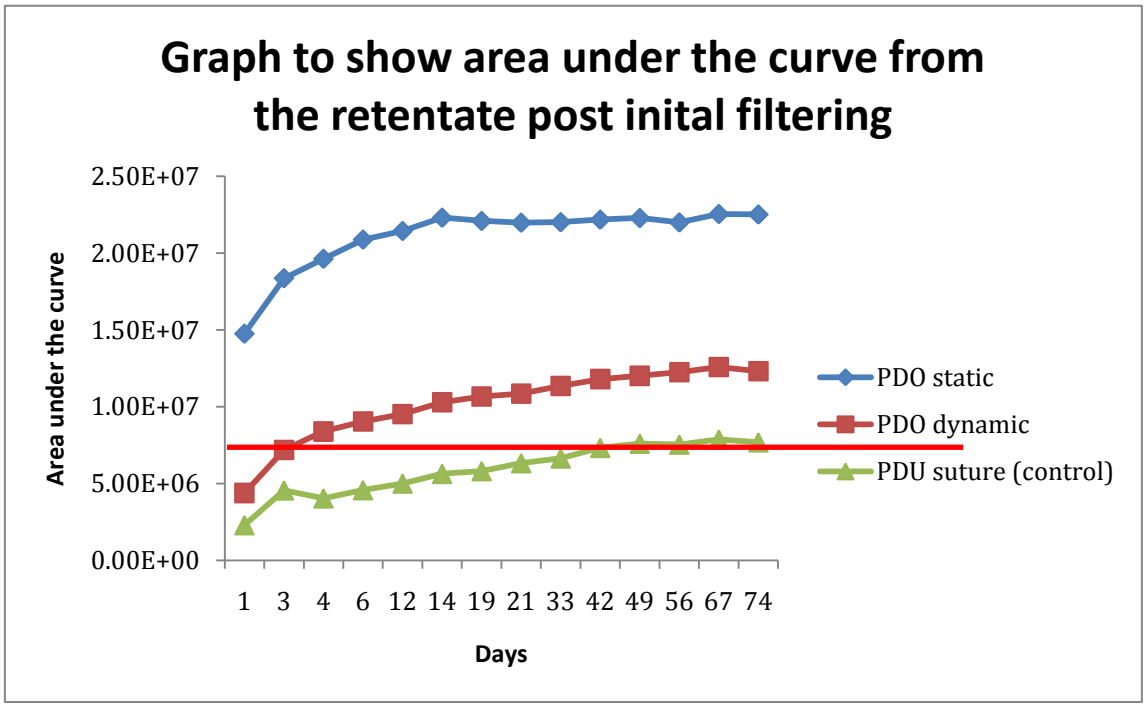


Figure 29: Cumulative HPLC signal generated from the retentate (in terms of areas under the peak). The straight line represents the position of the threshold of detection. Unlike Figure 28, here the concentrations of monomer gained from the retentate breach the threshold of detection.

3.4 Discussion

3.4.1 Weight loss and pH

There are two reasons why 4 weeks was used in this thesis as the appropriate length of time for the macrostructure of the patch to remain before it begins to significantly degrade. The first reason is that 4 weeks has previously been suggested to be the approximate duration for which cellular healing in the rotator cuff has the majority of its effect. Chen *et al,* for instance, found that up to 3 weeks after surgery, the gene expression and production of a variety of growth factors were up-regulated (44). Therefore in terms of the use of the PDO patch for the application as a biomaterial for tendon repair, the timings of the weight loss experiments were found to be appropriate (Figure 23). Similarly, the pH experiment showed a similar time frame before large changes were noted. The second reason why 4 weeks is appropriate is that once the benefit from any cells attached to the patch has been exhausted, it is important for the foreign material to be removed from the area in order to reduce further inflammation.

The results of the pH measurements confirmed the hypothesis that when the buffer is not replaced in the static experiment, the buffer capacity is exceeded and the pH falls as a result. Consequently, the pH of the static experiment is more acidic than that of the dynamic experiment, where pH was maintained above 6.

It is hypothesised that the continuous buffering seen in the dynamic experiment echoes the physiological situation better than the static experiment. Despite the rotator cuff being an area poorly perfused by a blood supply, the environment is still dynamic, with a constant blood and synovial fluid flow. The benefit of the static

experiment is an awareness of the lowest pH changes which can occur as a result of the PDO patch degradation *in vitro.* Along with the weight loss and HPLC experiments, it adds another dimension to our understanding of how electrospun PDO patches degrade.

3.4.2 Degradation mechanism using HPLC

It was of interest to characterise the patch in terms of the degradation mechanism and kinetics, because the degradation of the patch will provide a conduit for cells to be implanted into recovering rotator cuffs. The hypothesised action is as follows. As hydrolysis acts upon the polymeric fibres of PDO, pieces will detach. Many of these pieces will have cells attached which are subsequently recruited to the healing wound. In a similar fashion, the meshed fibrous network nature of the PDO patch is such that the polymer will provide no barrier to cells recruited to the wound by released growth factors. They will simply migrate through the pores. Imaging presented in Chapter 1 revealed the macro-structural changes undergone by the patch over time whilst incubated in PBS. On top of this macro-degradation, the aim of the HPLC experiments was to gain an understanding of the degradation not seen under the microscope. As much information as possible is needed about a biodegradable implant's degradation products before a product is introduced into humans. The molecular changes undergone are therefore important to identify. The safety profile of such a product would be incomplete without this information.

The results of the degradation kinetics HPLC experiment were interesting. As mentioned earlier, the material run through the HPLC apparatus after the initial filtration produced a signal below the detection threshold. It can therefore be

concluded that over the first 74 days, relatively little monomer (or final degradation product) is shed from the PDO patch. The signal does increase as the time points progress, however, since all five samples produce very similar signal strengths, this is likely due to accumulation of debris in the solution rather than a shedding of monomer.

The retentate samples, on the other hand, produce results that help to confirm the hypothesised degradation kinetics. With the Static experiment, the buffering qualities of the PBS are used up. Consequently, there is no buffer to balance the pH, and as a result the pH falls, causing a more rapid hydrolysis of the polydioxanone (15). This result is supported by the results of the pH experiment seen in Figure 24.

At first glance, these results seem to be in conflict with the hypothesis by Sabino *et al* that describes kinetically favoured hydrolysis on the amorphous regions occurring faster than the diffusion hindered attack on the crystalline lamellae (15). Our results demonstrate the contrary: large fragments from the diffusion hindered attack on the crystalline lamellae being produced early and more readily than the monomer from amorphous region hydrolysis. However, this interpretation does not take account of the cleavage-induced crystallisation described by Sabino *et al*. Initially, the amorphous regions are hydrolysed, with subsequent new crystal formation at the expense of shorter chains in the amorphous region. It can be surmised from our results that the monomer, or smaller polymeric fragments, produced by hydrolysing the amorphous regions (Route 1 of Figure 16:), accumulate in solution but were not at a concentration great enough to exceed the detection threshold of the HPLC apparatus. The larger fragments produced by hydrolysis of the crystalline lamellae, the volumes of which had

increased due to cleavage-induced crystallisation, were detected by the apparatus in significant volume. This indicates that the dominant initial degradation product is large polymeric fragments that are not small enough to pass through a 0.22nm filter.

The impact of larger polymeric fragments on the local tissue is an interesting topic that provides scope for further research. One hypothesis would be that larger polymers would be less acidic. Since acidity has been linked to an increased inflammatory response, these findings would suggest a safer implant than one whose degradation products were monomeric, more acidic, and more prone to induction of inflammation (45). Since one of the proposed roles of these implants is to recruit specialised cells for enhanced tendon repair, a degradation product that caused the influx of non-specific inflammatory cells would be akin to dousing a fire with petrol. There may be, however, a balance to be struck. A slow degradation of fibres could theoretically lead to fibrosis of an implant, which in this case would negate the aim of cell release. An overly rapid degradation releases more acidic breakdown products locally. The HPLC results indicate a constant release of larger polymeric fragments. This may help prevent stasis and subsequent fibrosis, as the degradation products are larger and less acidic than the final degradation product.

In Chapter 2, reference was made to bulk degradation versus surface erosion. The ESEM images suggested both of these occur at the same time (Chapters 2.3.1 and 2.3.2). These concepts are echoed by Sabino *et al* who described hydrolysis of the amorphous regions producing smaller fragments compared to attack of the crystalline lamellae which favoured production of larger fragments (15). The results from the HPLC help us to refine our understanding of these concepts further. Where before, the

assumption about surface degradation was that it involved largely monomeric molecules being produced, it can now be surmised that larger polymeric fragments are also produced by surface erosion. These were detected not by the initial filtrate HPLC assay, but by the retentate assay, since the initial fragments were too large to be filtered.

What implications does this have for the development of the PDO electrospun patch? With any implant, especially a biodegradable one, it is important to know what compounds are going to be released into the tissues over time. Much research has been done to investigate the potential dangers of, for instance, cobalt and chromium ions circulating in the blood following metal-on-metal hip resurfacing (40). This highlights the importance of knowledge about a material's properties, not least when this material is degraded and has the potential to circulate around the body and be deposited in distant organs.

The larger concentrations of material detected by the retentate experiment suggests that the most significant initial breakdown product is large polymeric fragments rather than a small α-hydroxy-acid. This in itself suggests that further experimentation on breakdown products needs to concentrate not only on the final monomer, but also, importantly, on these larger fragments that break off and can disperse into the bloodstream.

3.4.3 Identifying the degradation product

One specific purpose of the HPLC study was to confirm the findings of Lanza *et al* who stated that glyoxylic acid was the final breakdown product of polydioxanone (39). The

results from the HPLC apparatus do not confirm or reject this hypothesis because the 3 compounds used as comparisons to the breakdown products of polydioxanone produced very similar signals. Any attempt to distinguish between them would be statistically unreliable. What can be concluded, however, is that the breakdown product of polydioxanone is structurally very similar to lactic acid, glycolic acid, and glyoxylic acid. Further work is required to identify the exact structure of the breakdown product. Alternatively, as it is evident from the HPLC traces in Figure 25 that for each compound two peaks were generated, it is possible that these may represent two isomers of the same compound in solution. Thus, the results of this experiment raise the question of whether there is not one single final breakdown product, but instead a range, all of which were detected by our HPLC experimentation.

3.4.4 Limitation

There are limitations to the HPLC experiments. For instance, the chromatogram produced from a mixture of all four monomers did not produce four sets of peaks, thus indicating difficulty in distinguishing between structurally similar chemicals.

3.4.5 Further work

As research into the patch develops, it will be interesting to evaluate how cells that are incorporated into the patch respond to changes in the environmental pH. Hakimi *et al* have already demonstrated that the gradually degrading PDO patch is better than Vicryl for the use as a scaffold for cells, but with no conclusive evidence as to why this is the case (7).

Future work with HPLC could find optimal conditions in which to detect the smallest concentrations of the monomer with the highest accuracy. For instance, it would be

interesting to investigate what percentage of acetonitrile and water was optimal. Also, different solvents with different additives might yield higher powered results. Since this is not a much visited part of the science, there is much work to be done in this area.

Finally, determining the exact final degradation product of PDO in vitro, perhaps by an alternative method such as nuclear magnetic resonance (NMR), would be of great value.

4 References

1. Galatz LM, Ball CM, Teefey SA, Middleton WD, Yamaguchi K. The outcome and repair integrity of completely arthroscopically repaired large and massive rotator cuff tears. Journal of Bone and Joint Surgery-American Volume. 2004;86A(2):219-24.

2. Cummins CA, Murrell GAC. Mode of failure for rotator cuff repair with suture anchors identified at revision surgery. Journal of Shoulder and Elbow Surgery. 2003;12(2):128-33.

3. Derwin KA, Codsi MJ, Milks RA, Baker AR, McCarron JA, Iannotti JP. Rotator Cuff Repair Augmentation in a Canine Model with Use of a Woven Poly-L-Lactide Device. Journal of Bone and Joint Surgery-American Volume. 2009;91A(5):1159-71.

4. Derwin KA, Baker AR, Spragg RK, Leigh DR, Iannotti JP. Commercial extracellular matrix scaffolds for rotator cuff tendon repair - Biomechanical, biochemical, and cellular properties. Journal of Bone and Joint Surgery-American Volume. 2006;88A(12):2665-72.

5. Armstrong DG, Lavery LA, Diabet Foot Study C. Negative pressure wound therapy after partial diabetic foot amputation: a multicentre, randomised controlled trial. Lancet. 2005;366(9498):1704-10.

6. Sampson S, Gerhardt M, Mandelbaum B. Platelet rich plasma injection grafts for musculoskeletal injuries: a review. Current reviews in musculoskeletal medicine. 2008;1(3-4):165-74.

7. Hakimi O, Chaudhury S, Murphy R, Carr A. Differential growth on sutures of tendon cells derived from torn human rotator cuff. Journal of Biomedical Materials Research: Part B. In print.2011.

8. Getgood A, Bollen S. What tissue bankers should know about the use of allograft tendons and cartilage in orthopaedics. Cell and Tissue Banking. 2010;11(1):87-97.

9. Middleton JC, Tipton AJ. Synthetic biodegradable polymers as orthopedic devices. Biomaterials. 2000;21(23):2335-46.

10. Boland ED, Coleman BD, Barnes CP, Simpson DG, Wnek GE, Bowlin GL. Electrospinning polydioxanone for biomedical applications. Acta Biomaterialia. 2005;1(1):115-23.

11. Ray JA, Doddi N, Regula D, Williams JA, Melveger A. Polydioxanone (PDS), a novel mono-filament synthetic absorbable suture. Surgery Gynecology & Obstetrics. 1981;153(4):497-507.

12. Kricheldorf HR, Damrau DO. Polylactones, 42 - Zn L-lactate-catalyzed polymerizations of 1,4-dioxan-2-one. Macromolecular Chemistry and Physics. 1998;199(6):1089-97.

13. Maurus PB, Kaeding CC. Bioabsorbable implant material review. Operative Techniques in Sports Medicine. 2004;12(3):158-60.

14. Pietrzak WS, Sarver DR, Verstynen ML. Bioabsorbable polymer science for the practicing surgeon. Journal of Craniofacial Surgery. 1997;8(2):87-91.

15. Sabino MA, Albuerne J, Muller AJ, Brisson J, Prud'homme RE. Influence of in vitro hydrolytic degradation on the morphology and crystallization behavior of poly(p-dioxanone). Biomacromolecules. 2004;5(2):358-70.

16. Tracy MA, Ward KL, Firouzabadian L, Wang Y, Dong N, Qian R, et al. Factors affecting the degradation rate of poly(lactide-co-glycolide) microspheres in vivo and in vitro. Biomaterials. 1999;20(11):1057-62.

17. Athanasiou KA, Schmitz JP, Agrawal CM. The effects of porosity on in vitro degradation of polylactic acid polyglycolic acid implants used in repair of articular cartilage. Tissue Engineering. 1998;4(1):53-63.

18. Van Rijssel EJC, Trimbos JB, Da Costa A, Fleuren GJ, Brand R. Assessment of tissue reaction at suture knots: an adaption of Sewell's scoring system. European Journal of Obstetrics and Gynecology and Reproductive Biology. 1988;27(2):165-72.

19. Suganuma J, Alexander H. Biological response of intramedullary bone to poly-l-lactic acid. Journal of Applied Biomaterials. 1993;4(1):13-27.

20. Metz SA, Chegini N, Masterson BJ. Invivo tissue reactivityand degradation of suture materials - a comparison of Maxon and PDS. Journal of Gynecologic Surgery. 1989;5(1):37-46.

21. Kalfa D, Bel A, Chen-Tournoux A, Della Martina A, Rochereau P, Coz C, et al. A polydioxanone electrospun valved patch to replace the right ventricular outflow tract in a growing lamb model. Biomaterials. 2010;31(14):4056-63.

22. Costa P, Parsons M. New insights into the dynamics of cell adhesions. International review of cell and molecular biology. 2010;283:57-91.

23. Sabino MA, Feijoo JL, Nunez O, Ajami D. Interaction of fibroblast with poly(p-dioxanone) and its degradation products. Journal of Materials Science. 2002;37(1):35-40.

24. Baumann A, Burggasser G, Gauss N, Ewers R. Orbital floor reconstruction with an alloplastic resorbable polydioxanone sheet. International Journal of Oral and Maxillofacial Surgery. 2002;31(4):367-73.

25. Kontio R, Ruuttila P, Lindroos L, Suuronen R, Salo A, Lindqvist C, et al. Biodegradable polydioxanone and poly(L/D)lactide implants: an experimental study on peri-implant tissue response. International Journal of Oral and Maxillofacial Surgery. 2005;34(7):766-76.

26. Pietrzak WS. Principles of development and use of absorbable internal fixation. Tissue Engineering. 2000;6(4):425-33.

27. Wang EA, Rosen V, Dalessandro JS, Bauduy M, Cordes P, Harada T, et al. Recombinant human bone morphogenic protein induces bone-formation. Proceedings of the National Academy of Sciences of the United States of America. 1990;87(6):2220-4.

28. Ramchandani M, Robinson D. In vitro and in vivo release of ciprofloxacin from PLGA 50 : 50 implants. Journal of Controlled Release. 1998;54(2):167-75.

29. Ringe J, Kaps C, Burmester GR, Sittinger M. Stem cells for regenerative medicine: advances in the engineering of tissues and organs. Naturwissenschaften. 2002;89(8):338-51.

30. Danilatos GD. Review and outline of environmental SEM at present. Journal of Microscopy-Oxford. 1991;162:391-402.

31. Meredith P, Donald AM. Study of 'wet' polymer latex systems in environmental scanning electron microscopy: Some imaging considerations. Journal of Microscopy-Oxford. 1996;181:23-35.

32. Stokes DJ. Recent advances in electron imaging, image interpretation and applications: environmental scanning electron microscopy. Philosophical Transactions of the Royal Society of London Series a-Mathematical Physical and Engineering Sciences. 2003;361(1813):2771-87.

33. Cameron RE, Donald AM. Minimizing sample evaporation in the environmental scanning electron microscope. Journal of Microscopy-Oxford. 1994;173:227-37.

34. Dragnevski KI, Donald AM. An environmental scanning electron microscopy examination of the film formation mechanism of novel acrylic latex. Colloids and Surfaces a-Physicochemical and Engineering Aspects. 2008;317(1-3):551-6.

35. Chen CS, Alonso JL, Ostuni E, Whitesides GM, Ingber DE. Cell shape provides global control of focal adhesion assembly. Biochemical and Biophysical Research Communications. 2003;307(2):355-61.

36. Riley G. Tendinopathy - from basic science to treatment. Nature Clinical Practice Rheumatology. 2008;4(2):82-9.

37. Zong XH, Wang ZG, Hsiao BS, Chu B, Zhou JJ, Jamiolkowski DD, et al. Structure and morphology changes in absorbable poly(glycolide) and poly(glycolide-co-lactide) during in vitro degradation. Macromolecules. 1999;32(24):8107-14.

38. Fu BX, Hsiao BS, Chen G, Zhou J, Koyfman I, Jamiolkowski DD, et al. Structure and property studies of bioabsorbable poly(glycolide-co-lactide) fiber during processing and in vitro degradation. Polymer. 2002;43(20):5527-34.

39. Lanza RP, Langer RS, Vacanti J. Principles of tissue engineering. 3, Illustrated ed. Lanza RP, Langer RS, Vacanti J, editors2007. 1307 p.

40. Hart AJ, Skinner JA, Winship P, Faria N, Kulinskaya E, Webster D, et al. Circulating levels of cobalt and chromium from metal-on-metal hip replacement are associated with CD8+ T-cell lymphopenia. (vol 91, pg 835, 2009). Journal of Bone and Joint Surgery-British Volume. 2009;91B(12):1641-.

41. Qin W, Zhang YH, Li ZY, Dai YY. Extraction equilibria of glycolic and glyoxylic acids with trialkylphosphine oxide and trioctylamine as extractant. Journal of Chemical and Engineering Data. 2003;48(2):430-4.

42. Snyder L, Kirkland J, Glajch J. Practical HPLC Method Development. Second ed. USA: John Wiley and Sons, Inc.; 1997.

43. Latchman DS. Essential cell biology: An introduction to the molecular biology of the cell. Nature. 1998;393(6681):132-.

44. Chen CH, Cao Y, Wu YF, Bais AJ, Gao JS, Tang JB. Tendon Healing In Vivo: Gene Expression and Production of Multiple Growth Factors in Early Tendon Healing Period. Journal of Hand Surgery-American Volume. 2008;33A(10):1834-42.

45. Basic Cell Biology and Molecular Genetics. Biomolecular Action of Ionizing Radiation. 2008:21-50.